THE UNIVERSITY *of* EDINBURGH

Edinburgh Research Explorer

Fusion of remotely sensed displacement measurements: current status and challenges

OPEN ACCESS

Fusion of remotely sensed displacement measurements: current status and challenges

Y. Yan[1], A. Dehecq[1,2], E. Trouvé[1], G. Mauris[1], N. Gourmelen[2], F. Vernier[1]

1: LISTIC, Polytech Annecy-Chambéry, Université Savoie Mont Blanc, Annecy, France
Email: yajing.yan@univ-smb.fr
2: School of Geosciences, University of Edinburgh, UK

November 18, 2015

ABSTRACT

Nowadays, data fusion constitutes the key subject in numerous applications of remotely sensed displacement measurements, with the increasing availability of remote sensing data and the requirement of improvement of the measurement accuracy. This paper addresses the current status and challenges in the fusion of remotely sensed displacement measurements. An overview is given to discuss the remote sensing sources and techniques extensively used for displacement measurement and the recent development and achievement of displacement measurements fusion. Fusion between displacement measurements and integration of a geophysical model are discussed. The fusion strategies and uncertainty propagation approaches are illustrated in two main applications: 1) surface displacement measurements fusion to retrieve surface displacement with **reduced uncertainty** in case of redundancy, with larger spatial extension or of higher level in case of complementarity 2) surface displacement measurements fusion to estimate the geometrical parameters of a physical deformation model in case of redundancy and complementarity. Finally, the current status and challenges of remotely sensed displacement measurements fusion are highlighted. Moreover, some potential ways are proposed to deal with heterogeneous data types and to assimilate remote sensing data into physical models in order to realise near real time displacement monitoring.

1   Introduction

The surface of the Earth is deforming permanently due to mass transfer, either internal or external, either natural or man-made activities. The displacement at the Earth's surface vary a lot in terms of spatial

1

extension, amplitude and temporal evolution. The investigation of the displacement at the Earth's surface represents an essential part of geodesy and its quantification constitutes a major topic in the community of geoscience, since it is of particular importance for natural hazards monitoring. For example, the displacement measurements and the deformation model inferred from these measurements provide crucial information in order to avoid the installation of emergency shelter and reconstruction over affected areas that will result in further damage in a later earthquake [1, 2]. Further, these sources of information enrich the disaster early warning system in order to prevent the future natural hazards. Displacement measurements also present great potential for underground exploitation, bridges and dams sinking monitoring and they are of particular interest in civil engineering [**3, 4, 5, 6**].

At the end of the 20th century, the development of spatial geodetic techniques (optical & SAR imagery, GPS) has allowed for drastic improvement of the spatial coverage, the resolution and the accuracy of displacement measurements. **Spaceborne optical and radar sensors observe the Earth's surface continuously, across both space and time, but with limited flexibility in terms of revisit time and acquisition geometry. Airborne optical and radar sensors provide displacement measurements with limited spatial/temporal coverage, but improved flexibility in terms of revisit time and acquisition geometry. Moreover, ground based optical and radar sensors, with good flexibility in terms of revisit time and acquisition geometry, often give precise information for small scale phenomena.** Thanks to these techniques, spectacular results have been obtained in numerous applications with displacement of various characteristics in terms of magnitude, duration, spatial distribution, etc.: the study of subsidence in urban areas [**3, 7, 8, 9, 10, 11**], of the co-seismic, inter-seismic and post-seismic motions [12, 13, 14, 15, 16], of glacier flows [17, 18, 19], of volcanic deformation [20, 21, 22, 23], etc. Nowadays, the displacement maps obtained by remote sensing techniques reach an accuracy within millimetres per year for deformation velocity and cover almost the whole **land of the Earth**, including the non-instrumented remote areas and areas that do not have the necessary financial means and human resources for ground instrumentation. They have also proven very useful for regional studies. Moreover, due to the archiving system, a posteriori studies can be performed on areas where an interesting phenomenon has been detected. We thus have access to the initial phase. Therefore, remote sensing displacement measurements have obtained significant development in the past few years. They are considered as the predominant source for the detection and the quantification of the terrestrial deformation, from which geophysical models have been retrieved to further understand the deformation source in depth and the physical process that induces the displacement observed from the Earth's surface.

To this end, a good knowledge of the reliability of the remotely sensed measurements, as well as

of the geophysical models accordingly obtained, is crucial for all the researches and applications that use these sources of information. However, remote sensing displacement measurements are subject to incompleteness and uncertainty. Uncertainty is also present in the geophysical model due to limited knowledge about the phenomenon under observation and approximations made in the modelling, as well as uncertainties associated with the displacement measurements used to constrain the model. A perspective of significant **reduction in the uncertainty** of the displacement measurement appears thus with the increasing availability of different types of remote sensing measurements and the blooming development of displacement information extraction techniques. Thereby, the role of data fusion, making use of the redundant and complementary displacement information brought by different sources, becomes more and more important. Methodological development of the fusion of different types of displacement measurements and of the integration of a physical model based on supercomputer facilities seems necessary to improve the spatial extension and the accuracy of displacement measurements. In this context, this paper addresses the current status and challenges of the fusion of remotely sensed displacement measurements.

This paper is organised as follows: In Section 2, remote sensing sources including optical, SAR images, in situ GPS measurements and levelling sources, as well as displacement extraction techniques such as offset-tracking, differential interferometry (DInSAR) are introduced. Moreover, the uncertainty quantification of measurements issued from these techniques is also discussed. In Section 3, the fusion of displacement measurements and the integration of geophysical models are presented. The fusion issues are presented through 2 main applications: from raw measurements to fused measurements and from measurements to model parameters. Finally, in Section 4, the current status and challenges are highlighted and perspectives to deal with heterogeneous data types and to assimilate remote sensing data into physical models are proposed.

2 Displacement measurement data

Nowadays, SAR and optical images constitute the predominant remote sensing source for displacement measurement, due to their high capacity in providing displacement measurement over large area and of great accuracy. GPS and levelling measurements, thanks to their high **precision**, are also widely used as complementary sources to **remote sensing data**.

2.1 Displacement extraction techniques

Two different families of technique have been developed to extract displacement information from SAR or optical images: offset-tracking of amplitude SAR or optical images and DInSAR. Techniques in the family of offset-tracking, based on the cross-correlation between the master image and the slave image, provide two dimensional (2D) measurements (namely correlation measurements hereafter), with one horizontal component in the direction of the sensor motion and the other component in the perpendicular direction in the horizontal plane for optical images and in the Line Of Sight (LOS) for SAR images. The accuracy of these techniques is limited by the resolution of the images used, the stereoscopic effect and the decorrelation. Numerous studies have confirmed that the displacement error is generally included between tenth of pixel and one pixel [24, 25]. The best accuracy obtained is recorded as 1/30 pixel for SAR images [26] and 1/200 of pixel for optical images [27] with careful data processing. **The application of offset tracking techniques is thus mainly determined by the resolution of the images used and the magnitude of the displacement to measure. Therefore, they are commonly applied for large displacement, e.g.** glacier flow monitoring [28, 29, 30, 31] and strong earthquake measurement in the field near the fault rupture [**24, 12, 32, 33, 34, 35**].

DInSAR, on the other hand, makes use of the phase information included in a pair of SAR images and allows for the measurement of the displacement occurred between the two acquisitions in the LOS direction. Compared to offset-tracking, this technique requires **strong coherence between two SAR images, for which the geometrical and temporal baselines between the two acquisitions should be as small as possible. Moreover,** more complex processing steps such as the orbital, topographical and atmospheric correction and phase unwrapping **are necessary**. In particular, phase unwrapping determining the success of the application of DInSAR, is difficult and delicate since the choice of the phase unwrapping method depends on the nature of the interferograms to be processed. The problems mainly encountered are the discontinuity of the coherent areas and the strong gradient of the displacement that can cause potential aliasing problem. Today, no method seems fully operational. DInSAR has been widely used to measure small displacements such as surface subsidence in urban area [7, 36, 37, 8], inter-seismic deformation [14, 38, 16] or glacier flow [39, 40, 41, 18], with an average accuracy of centimetres. With the increasing availability of SAR images, techniques such as Permanent Scatterer (PS) [42, 43, 44, 45] and Small BAseline Subset (SBAS) [**46, 47, 48, 49, 50**] dealing with time series have been developed in order to **reduce the uncertainty** of the displacement measurement and to get around of the principal limitations of the conventional DInSAR technique. With these techniques **and the availability of the X-band high resolution images (TerraSAR-X, COSMO-SkyMed)**, **precision** on the order of millimetres per year

has been obtained for displacement rate. Recently, combination of these two techniques is performed in order to further **reduce the uncertainty** of the displacement measurements and promising results have been obtained [51, 52, 9]. **Furthermore, multiple aperture InSAR (MAI) technique, based on split-beam InSAR processing, has been developed in order to extract along-track displacement from DInSAR data [53, 54]. The along-track displacement obtained is consistent with that obtained from offset-tracking. Note also that, in multitemporal InSAR processing, the deformation velocity estimation can be strongly biased by the thermal dilation of the imaged objects. Improvement of existing approaches and development of new approaches [55, 56, 57] have been proposed to deal with this issue. With these approaches, it is possible to achieve an extremely accurate monitoring of thermal dilation, up to a sensitivity on the order of 1 mm in the deformation measurement [56].**

Besides SAR and optical images, continuous GPS, as a complementary remote sensing source, is also widely used in displacement measurement. Different from SAR/optical imagery, GPS provides the 3D displacement (with 3 components: East, North, Up in the terrestrial reference) on a much sparse and irregular spatial grid with temporal sampling every 5 minutes or even less. The uncertainty associated with the GPS displacement measurement is sufficiently small, on the order of 5 - 10 mm and 10 - 20 mm in horizontal and in vertical respectively [58]. Thanks to the dense temporal sampling, GPS allows us to obtain time series for displacement varying over time, at the scale of days and years. GPS measurements have been used in detection of tectonic activities like earthquake [59, 15]), volcano [60], glacier flow [61], plate movement [62], etc. Moreover, levelling, the measurement of elevation difference between 2 points at the Earth's surface, can also be considered as a precise method for vertical displacement measurement. It has been used for displacement measurement for more than half a century [63, 64, 65, 15]). **A precision** on the order of mm/yr has been reported for vertical displacement rate [66]. However, besides the punctuality of the measurement, the major disadvantages of levelling also include the high cost and the large amount of time needed for collecting the data over long distances or over a large network.

2.2 Uncertainty quantification

The sources of uncertainty in optical/SAR imagery are very complex: they come from different perturbations that take place along the electromagnetic wave propagation (e.g. atmosphere) and at the backscattering surface (e.g. properties change during two acquisitions), as well as the noise generated in the electronic processing. Moreover, imperfect displacement extraction technique (accuracy of the algorithm) and pre/post-processing treatment (coregistration, geometrical correction, etc) also induce uncertainties

in the displacement measurement. The sources of possible uncertainty in GPS measurements come from the atmospheric effects, the measurement noise or distortion of the signal caused by electrical interference or errors inherent in the GPS receiver, clock drift, etc. These diverse sources results in uncertainties with very complex characteristics. In addition, the ground truth is not available in most cases of terrestrial deformation. For all these reasons, the quantification of the uncertainty **and the accuracy** associated with the displacement measurement still remains a delicate problem.

For feature-tracking measurements from optical/SAR images, two methods exist in the literature to estimate the displacement uncertainty. The first method adopts parameters associated with the correlation algorithm, for example, the correlation peak, the full width at half maximum, the curvature of the correlation surface, to represent the displacement uncertainty [67]. This kind of parameters indicate the relative reliability of the displacement measurement, they are thus not a measure of the uncertainty in strict sense. The second method consists of estimating a statistical variance in known stable areas [29, 68]. With this method, the spatial distribution of uncertainty is not available, since only one value is estimated for one pair of image. With large data sets, however, it is possible to statistically estimate the uncertainty at each point [19]. In case of earthquakes, pre-seismic image pairs are often used. This kind of uncertainty characterises essentially the random variation of the displacement, it cannot represent systematic and spatially correlated uncertainties. For DInSAR measurements, the main sources of uncertainty are considered from phase unwrapping. In [69, 7], phase unwrapping errors are analysed through the misclosure of the interferograms networks, given that the redundancy exists between the interferograms used. In [70], the variance of the phase is estimated from the coherence. This variance can only represent the random part of the uncertainty due to the presence of random noise in the interferogram. In [71, 72, 16],**the spatially correlated error is characterised in areas where neither deformation signal is expected nor visible on the interferogram assuming stationary and isotropic noise. For this, the semi-variogram and the semi-covariogram are computed as follows:**

$$\hat{\gamma}(h_c) = \frac{1}{2N} \sum_{i=1, \|r_i - s_i\| \simeq h_c}^{N} [d(r_i) - d(s_i)]^2 \tag{1}$$

$$\hat{C}(h_c) = \frac{1}{2N} \sum_{i=1, \|r_i - s_i\| \simeq h_c}^{N} d(r_i) \cdot d(s_i) \tag{2}$$

where $\hat{\gamma}$, $\hat{C}$ are the discrete sample semi-variogram value and the discrete sample semi-covariogram value for distance h_c. N is the number of data points pairs at locations r_i and s_i such that $\|r_i - s_i\| \simeq h_c$. d **is**

the displacement value measured in interferograms.

With respect to the previous approaches, the advantage of this approach lies on the consideration of the spatially correlated error which constitutes an important part of the uncertainty that should be taken into account, since this part of uncertainty almost always exists in the interferogram due to the atmospheric and topographic effects.

GPS measurements are often repeated observations and they are assumed to be samples of stochastically independent normally distributed random variables. The variability of the samples, the standard deviation, is often used as uncertainty associated with the displacement measurement. More elaborated analyses are described in [73]. The vertical displacement measured by levelling are also supposed to be samples of stochastically independent normally distributed random variables. The variance of the displacement can be deduced from the combination of the variance of the reference point (point without displacement, the absolute displacement is determined with respect to this point) and that of the elevation differences [74]. The standard deviation is used as the uncertainty associated with the displacement. A more elaborated method to estimate the complete covariance matrix for levelling measurements is proposed in [75].

3   Fusion of displacement measurements

Fusion constitutes a formal framework in which are expressed the means and techniques that allows for the combination of information from diverse sources. The general principle consists of associating various information on the same problem in order to improve the knowledge. The imperfection of individual information such as the uncertainty, the incompleteness, the ambiguity, etc, constitutes the primary motivation of the fusion. Depending on the phenomenon under consideration, different fusion strategies are necessary to reduce the imperfection of individual information, benefiting the redundancy and the complementarity of one source of information with respect to the others. In displacement measurement, **the main imperfection to be improved by the fusion includes: 1) incompleteness due to limitations of data acquisition and/or data processing 2) uncertainty due to noise from data acquisition until the final displacement results**.

3.1   Fusion between displacement measurements

Remote sensing measurements mainly provide displacement information at the Earth's surface. Currently, the fusion of these surface displacement measurements can be summarised into 2 groups according to the

objectives. The first group corresponds to the processing "from raw measurements to fused measurements". In case of redundancy, the surface displacement measurements are combined to retrieve a surface displacement with **reduced uncertainty**. In case of complementarity, they are combined to retrieve a surface displacement with larger spatial extension or of higher level (for example, the 3D displacement field). The second group corresponds to the processing "from measurements to model parameters". Surface displacement measurements are combined to estimate the geometrical parameters of a physical deformation model in case of redundancy and complementarity.

3.1.1 From raw measurements to fused measurements

In case of redundancy, the common and intuitive approach consists in averaging all available measurements in order to obtain an estimation as **precise** as possible [76, 77, 78, 79]. However, this approach is subject to the difficulty in determining the contribution of each measurement and to the limitation of computational capacity while dealing with large volume data sets. Figure 1 gives an example of interferograms stacking for displacement measurement on the Hayward fault in the San Francisco Bay Area from 1992 to 2000 [78]. For this, 37 interferograms with spatial baseline less than 200 m and temporal baseline longer than 1 year are selected. This set of 37 interferograms are stacked by dividing the cumulative range change by the cumulative time span, which preferentially weighs the range change rate of those interferograms with longer temporal baseline. Afterwards, interferograms where more than 5% of the coherent phase exceeds 3 standard deviations from the stacked results are removed. Finally, a subset of 13 independent interferograms are selected for the stacking and the standard deviation is used as uncertainty measure associated with the stacked range change rate. Thanks to this stack, the atmospheric artefacts in individual interferograms are reduced significantly.

[Figure 1 about here.]

In case of spatial complementarity, a mosaic is usually performed in order to obtain a displacement measurement over large area. This is very useful to generate displacement maps at global scale [18, 68, 19]. Figure 2 shows the annual velocity field obtained from feature-tracking of Landsat images to measure glaciers flow over the Karakoram. Panel (a) shows the result for a single pair (the pair with the highest spatial coverage among all available pairs): many gaps appear in saturated areas or areas covered by clouds (corresponding to measurements with a signal-to-noise ratio below 4), limiting the percentage of estimates over glaciers to 70%. Velocities in stable areas, expected to be null, are in the range of 10 m/year due to orthorectification errors. On the other hand, panel (b) shows the velocity obtained from fusion of 29

annual pairs available for the period 1999-2001 and taking the median value at each location. The spatial coverage is increased to 94% thanks to the complementarity from one pair to another. Velocities in stable areas are reduced to 2.0 m/year thanks to the redundancy, and because orthorectification errors are not coherent [19].

[Figure 2 about here.]

In case of temporal complementarity, measurements time series can be used to follow the temporal evolution of the event with appropriate method, such as PS and SBAS approaches [**46, 42, 43, 50, 80, 44**]. These approaches have been modified and improved since their first applications. Variants of SBAS approach such as PO-SBAS [26] and PSBAS [81] have been developed in order to **make use of pixel offset measurements** and to deal with large data sets. Variant of PS approach such as SqueeSAR [82] has been developed in order to improve the performance of the PS technique proposed previously. **Along with PS interferometry, SAR tomography based approaches allow for an improvement in the detection of permanent scatterers in urban areas [83, 84, 85, 86, 87].** Figure 3 gives an example of surface displacement time series obtained with SBAS [50] and PO-SBAS [26] for Fernandina and Sierra Negra. The temporal evolution of the surface displacement for these two calderas is characterised thanks to the temporal complementarity. The eruptions for both calderas have been well identified by the abrupt change of the displacement magnitude from the time series. Regarding the quantification of the uncertainty associated with the displacement time series, it constitutes a truly complex task. For PS approaches, because of the iterative process (including the temporal phase unwrapping and the spatial integration) adopted by most PS approaches, the propagation of the input uncertainty and the quantification of the final uncertainty seem extremely difficult. The phase standard deviation is usually used as an indicator of the quality of the displacement velocity obtained. However, this parameter is strongly related to the nonlinear motion according to [51], thus not an appropriate indicator of the displacement uncertainty. For SBAS approaches, the main difficulty also lies on the quantification of the phase unwrapping error. In [7], the RMS misclosure is calculated to assess the phase unwrapping quality, but no clear uncertainty associated with the final displacement time series is provided.

[Figure 3 about here.]

In case of geometrical complementarity (from diverse acquisition geometries: different incident angles, different orbital directions (descending and ascending), different displacement directions (range and azimuth)), the 3D displacement at the Earth's surface is usually retrieved by a linear inversion in least

9

square sense in order to interpret the surface displacement field in an homogeneous and intuitive way [40, 88, 89, 12, 90]. For example, in the displacement measurement of the Kashmir earthquake in 2005, surface displacement measurements from correlation of SAR amplitude images and DInSAR, including ascending and descending passes and different incident angles, are available. Both redundancy and spatial and geometrical complementarity thus exist. In particular, correlation and DInSAR measurements issued from the same pair of SAR images are available and these two types of measurements provide essentially complementary displacement information. On one hand, correlation measurements are reliable in areas where the displacement is large (usually close to the deformation source), while DInSAR measurements are mainly available in areas where the displacement is small (usually far from the deformation source). On the other hand, besides the displacement measurement in LOS direction, correlation measurements provide displacement measurement in azimuth direction, which is complementary to the DInSAR measurements. Regarding the redundancy of displacement measurement in LOS direction provided by both measurements in areas of moderate displacement, correlation measurements can be used to check the existence of phase unwrapping error and to retrieve the absolute displacement value in DInSAR measurements since relative displacement value is obtained from the phase. Further, since the **precision** of DInSAR measurement is much higher than that of correlation measurements, the contribution of DInSAR measurement is naturally more significant than that of correlation measurements.

For the Kashmir earthquake (2005) example, 23 surface displacement data sets are available in total. Two fusion strategies, namely joint inversion and pre-fusion are investigated together with two uncertainty propagation approaches: one based on the probability theory and the other based on the possibility theory [91, 92]. In joint inversion, all available measurements are used simultaneously in the inversion. Pre-fusion consists of a fusion step before inversion. This fusion step can be performed for example using the mean value, the median value of a set of measurements or by selecting the best one according to certain criteria, for example, the reliability of measurements or the signal-to-noise ratio. Afterwards, the refined data sets are input in the inversion. In the probabilistic approach, displacement errors are assumed random and independent (optimist hypothesis that cannot be justified in most cases). They are represented and propagated by Gaussian distributions. With this hypothesis, the more measurements are fused, the smaller the output uncertainty is. The solution (displacement value U and displacement uncertainty Σ_U) given by the least squares inversion is shown in equation 3.

$$U = (P^t \Sigma_R^{-1} P)^{-1} P^t \Sigma_R^{-1} R$$

$$\Sigma_U = (P^t \Sigma_R^{-1} P)^{-1} \tag{3}$$

where U denotes the 3D displacement vector with 3 components. P is the projection vector from the 3D displacement to displacements measured by correlation and DInSAR. **It is determined by the acquisition geometry:** $P_{LOS} = (-cos\varphi sin\theta, sin\varphi sin\theta, -cos\theta)$, $P_{azimuth} = (sin\varphi, cos\varphi, 0)$ **with** φ **azimuth of the satellite trajectory and** θ **the incident angle.** R corresponds to the vector of displacement measured by correlation and/or DInSAR. Σ_R and Σ_U represent the error covariances of R and U respectively.

In the possibilistic approach, no hypothesis is made on the displacement errors and they are represented and propagated by possibility distributions. The output uncertainty takes into account the worst bound among all the fused measurements (pessimist approach). As a result, even with more measurements, the output uncertainty is not decreased. The solution (possibility distribution $\widehat{U}$ including the displacement value and the displacement uncertainty at the same time) given by the least squares inversion is shown in given by:

$$\widehat{U} = (P^t \Sigma_R^{-1} P)^{-1} P^t \Sigma_R^{-1} \otimes \widehat{R} \tag{4}$$

$\widehat{U}$ denotes the possibility distribution of the 3D displacement vector. $\widehat{R}$ corresponds to the possibility distribution of the vector of displacement measured by correlation and/or DInSAR. ^{t} denotes the transpose and $\otimes$ refers to the matrix operator of fuzzy multiplication where the sum and the conventional scalar product are replaced by the corresponding fuzzy operations (**min and max operators in most cases**) [**93, 91**].

An example of the Up component of the 3D displacement and the associated uncertainties is given in Figure 4. With the probabilistic approach, compared to pre-fusion, the uncertainty is reduced in areas where more measurements are available in joint inversion, while with possibilistic approach, the uncertainty is increased in the same areas, because of a different approach of uncertainty propagation. According to further demonstrations and analyses in [94], authors concluded that with both fusion strategies, the uncertainties associated with the 3D displacement field are reduced by fusion. On one hand, when random uncertainties are present in the measurements, the strategy of joint inversion can most reduce the uncertainty and the probabilistic approach is appropriate to represent and propagate the uncertainty. On

the other hand, when systematic uncertainties are present in the measurements, the strategy of pre-fusion gives better results and the possibilistic approach seems appropriate to represent and propagate the uncertainty. In addition, the strategy of pre-fusion is computationally more efficient than the strategy of joint inversion. In most real cases, random and systematic uncertainties are often present simultaneously in the displacement measurements. The uncertainty associated with the 3D displacement obtained with the probabilistic approach provides a lower bound, whereas that obtained with the possibilistic approach provides an upper bound. The real value should be situated in between. When random uncertainty is the main source of uncertainty in correlation/DInSAR measurements, the 3D displacement uncertainty is closer to the probabilistic result (equation 3). On the contrary, when systematic uncertainty dominates the uncertainty in correlation/DInSAR measurements, the 3D displacement uncertainty is closer to the possibilistic result (equation 4).

[Figure 4 about here.]

3.1.2 From measurements to model parameters

One of the most important objectives of geophysics is to estimate, from surface displacement measurements, the geometry and the force of the deformation source in depth, e.g. a fault rupture and the associated slip in case of an earthquake or of a magmatical intrusion and an opening in volcanic context. Fusion of SAR, optical displacement measurements, GPS and other sources of information to constrain a physical model, such as the Okada model [95] and the Mogi model [96], by linear/nonlinear inversion thus constitutes a major topic in displacement measurement. In this case, spatial and geometrical complementarity is very important to infer model parameters correctly, because trade-off between model parameters exists and some parameters are only sensitive to surface displacements in a certain area or in a certain direction. Partial displacement information thus results in erroneous model parameters estimation. Because of the complexity of the model inversion, the fusion processing, especially the uncertainty propagation is much more complicated than in the previous case. The common fusion strategy is the joint inversion using all of the available surface displacement measurements. For sake of computational efficiency, surface displacement measurements are often subsampled in quadree so that the measurement point distribution varies as a function of the displacement gradient [97, 98, 99, 78].

3.1.2.a   Fusion of same type displacement measurements

In case of displacement measurements of the same type, SAR or optical measurements alone, the fusion strategy of pre-fusion, for example selecting highest quality measurements among all of the available measurements, can provide better results, given that good agreement cannot be obtained between all the measurements and the selected high quality measurements include almost all the useful information. In the case of the Kashmir earthquake (2005), a fault rupture model is inferred from the selection of high quality SAR measurements and this model cannot be obtained with the strategy of joint inversion. Artefact **(erroneous slip with large magnitude situated at 40-50 km and 80-90 km along strike distance)** exists in depth **(deeper than 20 km along dip distance)** using all of the available measurements as shown in Figure 5. Because of the noise present in the measurements, it is easier to adjust a model to a small number of measurements of high quality, but covering sufficient displacement information.

[Figure 5 about here.]

Regarding the uncertainty propagation, the approach commonly used consists of performing a large number (hundreds to thousands) of noise realisations in the surface displacement measurements and running repeatedly the model inversion in order to obtain the distribution and the correlation of model parameters [100]. An example is shown in Figure 6. The uncertainty associated with each model parameter is characterised by the histogram and the correlation between parameters is represented by the scatterplot. In this way, the uncertainties of the input measurements are propagated to the model parameters through the model functionality. However, note that uncertainty already exists in the input measurements before the noise realisation. Therefore, double levels of uncertainty exist in the measurements after the noise realisation. Uncertainties associated with the model parameters accordingly obtained thus do not represent the real uncertainties. They rather reveal the sensitivity of the model to noise. In practice, this approach is not always applied because of the computational cost. Instead, the quality of the retrieved model is evaluated directly by the residual compared to the measurements used in the model retrieval in some works [89, 100, 12, 34].

[Figure 6 about here.]

3.1.2.b   Fusion of different types displacement measurements

In case of heterogeneous measurements with diverse characteristics and **uncertainties**, the fusion processing can be very complex. **There have been numerous investigations that combine GPS and InSAR data to optimally measure coseismic deformation [98, 97, 99, 72, 101, 102, 103, 104], interseismic deformation [105, 38], post-seismic deformation [106, 107, 108] and volcanic deformation [109].** The major difficulty lies on the determination of the relative contribution of each measurement. In general, the weight of each measurement depends on the associated uncertainty. For one data set, we can determine the contribution of each measurement according to their associated uncertainty. However, it is very difficult to provide a link between the measurements of one data set and the measurements of another data set of different type. In other words, we usually have information about the error covariance between measurements inside one data set (namely the first level weighting hereafter), but we do not have information about the error covariance between different data sets (namely the second level weighting hereafter), the full covariance matrix of error is thus unknown. The relative contributions of different data sets are often decided in an arbitrary way. **For example**, in [98, 99, 72], only the first level weighting was taken into consideration, on the basis of the uncertainty associated with displacement at each pixel. In [97, 78, 38], the two levels of weighting are performed. The relative contribution of each data set was determined by minimising the residual of all the types of measurements. For this, first sets of relative weight obtained from separate inversions with different types of data are necessary. An example for the latter (the two levels of weighting) is given in Figure 7. The slip models for the slow slip events in 2006 in the Guerrero seismic gap inferred from GPS and DInSAR measurements separately and jointly are shown. According to [38], the model obtained from one data type alone cannot explain well the displacement behaviour observed from the other data type and the joint minimisation of the residual of both GPS and DInSAR measurements allows for better constrain of the slip model, since the displacement behaviours observed from both data types are taken into account.

[Figure 7 about here.]

However, in this way, the uncertainty associated with each data set is not really taken into account. For a data set whose uncertainty is larger, it is normal that the corresponding residual is larger. Moreover, if the phenomenon under consideration is more sensitive to the horizontal displacement than to the vertical displacement, naturally the model to be adjusted takes more contributions of the measurements in the East and North directions of GPS data sets into account. This can cause a larger residual for the measurement in the LOS direction of DInSAR data sets. Therefore, the approach based on the joint minimisation of

14

residual is not appropriate in some cases. A potential way to avoid the disadvantages mentioned previously consists in constructing the full covariance matrix of error from a large number of noise realisations, inspired from the principle of the Ensemble Kalman Filter [110]. Regarding the uncertainty propagation in this case, the approaches of the noise realisation and the residual comparison mentioned previously (section 3.1.2.a) are used [98, 97, 72].

3.2 Integration of geophysical model

Besides the displacement measurements, the deformation model also provides useful displacement information, especially when displacement measurements are not available over some areas or during some periods. Fusion between the measurements and the predictions of the model in different manners has also been reported in previous works [78, 7, 111, 34].

3.2.1 Model prediction for displacement measurement extraction

The model prediction can be used to aid the displacement measurement extraction. The a priori information provided by the model can be considered as a guide for the displacement measurement extraction. For example, in SAR imagery, the deformation model can be used to facilitate the phase unwrapping, even though the displacement predicted by the model is not perfectly accurate. With the displacement predicted by the model removed from the interferogram, the number of fringes can be reduced, which makes the phase unwrapping easier, especially when the displacement gradient is large. In [78], a deformation model constrained by GPS data is used to remove the displacement from each interferogram. In [7], a deformation model is obtained from stacking the 5 best interferograms, then the phase unwrapping is guided by this deformation model. **In [112], the smoothed range offset is used as a proxy for interferogram phase.** In the previous works, it is much easier to unwrap the residual (original interferogram - deformation model) instead of unwrapping the original interferogram. In this way, the phase unwrapping error is reduced significantly. In [111, 34], authors estimated the displacement field with the help of a mechanical deformation model and used multi-scale local frequencies of the phase (phase gradient) for phase unwrapping. Thanks to this method, the DInSAR has been applied successfully for the first time in displacement measurement of the Kashmir earthquake (2005). An example of this approach is shown in Figure 8. The deformation model in LOS direction corresponds to the surface displacement predicted by an homogeneous elastic linear deformation model obtained from the coseismic slip distribution in [12]. From this model, the optimal scale (number of multi-looking), at which the phase unwrapping can be

15

performed in keeping the best resolution and avoiding the aliasing problem at the same time, is estimated. Thereafter, on one hand, phase unwrapping is carried out using the multi-scale local frequencies of the phase with a global least squares method. On the other hand, the wrapped interferogram is filtered by the multi-scale local frequencies of the phase in order to highlight the fringe patterns. Finally, the residual, calculated by comparing the re-wrapped unwrapped phase to the filtered phase, is quantified to validate the results. Only the interferograms whose residual is inferior to 2π are considered as correctly unwrapped.

[Figure 8 about here.]

3.2.2 Joint use of model prediction and displacement measurement

The measurements and the model prediction can be used jointly to obtain some displacement information with improved quality or some displacement information that cannot be obtained with the measurements or the model alone. In [34], authors proposed a 2-segment fault rupture model that fitted better the observations than other 1-segment models obtained in previous work. This 2-segment model is inferred based on the surface displacement measurements and a 1-segment model obtained in the previous work [12]. With either the measurements or the 1-segment model alone, it is impossible that this 2-segments model can be retrieved. In [15], the coseismic and post-seismic slip distributions on the Paganica fault and the Campotosto fault of the 2009 L'Aquila earthquake are obtained based on the Paganica fault rupture plane geometry estimated in [113] and the Campotosto fault geometry derived from geological mapping studies (Figure 9). Small translation and rotation are performed to the modelled fault plane geometry in order to make it consistent with the observed surface rupture. The coseismic and post-seismic slip distributions are estimated based on these fault geometries and using DInSAR, GPS and levelling measurements. Indeed, for a given event, the fault geometry and slip distribution models in the previously published works often provide useful information for similar works later. **Moreover, [114, 115] used jointly wrapped interferograms and geophysical deformation models to estimate the fault rupture parameters, avoiding the phase unwrapping which constitutes a major problem in interferometric processing.** In addition, the measurements and the physical model can be combined together in a dynamic context to follow the temporal evolution, even to predict the future behaviour of the phenomenon under observation, which corresponds to the data assimilation that is commonly used in atmosphere and ocean science and has gained more and more attention in geoscience. In [116], the DInSAR surface displacement measurements are combined with a geomechanical model to characterise the evolution of the underground gas storage and to reduce the uncertainty associated with the model parameters.

16

3.3 Discussion

In displacement measurement, data fusion is often realised by linear and/or nonlinear inversion. In general, a consistency check is necessary before data fusion. It constitutes an important step that allows for an identification of the possible conflict between different measurements, then of the possible aberration present in some measurements. The latter should be removed in the data fusion process in order not to degrade the quality of the fusion results. Moreover, an analysis of the redundancy and the complementarity between different measurements is of particular importance to provide useful information for the choice of the fusion strategy. Furthermore, the characterisation of the displacement uncertainty is also essential for the choice of the appropriate fusion strategy. However, the uncertainty quantification investigation seems insufficient currently. In many studies, the detailed description of the displacement uncertainty is not available.

In case of redundancy, if random uncertainty is present in the individual displacement measurement, all the measurements can be used jointly in linear inversion in order to maximise the reduction of the uncertainty associated with the fusion results, given enough computational capacity. For nonlinear inversion, the performance of this strategy depends on the data quality (noise level). This strategy can fail when it is difficult to adjust a model among a large number of noisy data. If systematic uncertainty is present in the individual displacement measurement, the pre-fusion can be a good choice for both linear and nonlinear inversions. An appropriate fusion step before the inversion allows reducing most the systematic uncertainty. In case of complementarity, since each individual measurement brings non-replaceable information, all the measurements should be used. In both cases of redundancy and complementarity, data fusion can provide optimal results only if the specification of the displacement uncertainty is appropriate.

In practice, both redundancy and complementarity exist in most studies. Moreover, the uncertainty associated with each measurement is not always reliable, even unavailable in some cases, which makes the judgement of the agreement between different measurements difficult. Currently, the main topic on displacement measurement fusion consists of using as many measurements as possible, joint inversion is thus the most used fusion strategy with expectation that we can obtain new information using more measurements. With good data quality (random uncertainty of small amplitude), this strategy can give satisfactory results, while with moderate or poor data quality (random uncertainty of large magnitude of systematic uncertainty), this strategy can fail because, it is difficult, on one hand, to adjust a model

17

among many noisy data, on the other hand, to determine the appropriate relative contribution of each measurement, even though numerous studies have been focused on the search of the optimal weighting of heterogeneous measurements. In this case, pre-fusion can be considered as a good choice. In case of complex geophysical model inversion where the computational time is the main concern, a step of pre-fusion between redundant measurements before the inversion is also preferred in order not to burden the inversion system.

4 Conclusions and perspectives

The arrival of remote sensing has caused a true revolution in displacement measurement by significantly improving the spatial coverage and the measurement accuracy. Spectacular results have been obtained in numerous fields: the study of urban subsidence, of coseismic, inter-seismic and post-seismic motion, of glacier flow, of volcanic deformation, etc. With the continuous launching of Earth observation satellites and the increasing availability of the amount of remote sensing data, data fusion becomes necessary and plays a more and more important role in displacement measurements. However, using all of the available measurements cannot always provide satisfactory results, but always presents difficulties such as unknown weighting coefficients and high computational cost. Intelligent fusion strategies and methods, involving how to benefit from the large volume of data in an efficient way to reduce the displacement uncertainty and to improve our knowledge on the physical process of the phenomenon under observation, constitutes a living topic in many works. Meanwhile, more and more attention is paid to the displacement uncertainty characterisation and quantification. The consideration lies not only on independent random uncertainty but also on correlated or systematic uncertainty. The uncertainty management approach has also been extended from a probabilistic approach to a possibilistic approach. On the other hand, the techniques in displacement measurement by remote sensing are still being improved in order to integrate as much as possible the benefit of the high spatial resolution and the increasing frequency of data acquisition for terrestrial displacement measurements. Moreover, efforts have been made to combine different techniques, for instance, the combination of PS and SBAS methods, of correlation and DInSAR, seeking to make the best use of the information contained in the data by exploiting the complementarity of different techniques.

Besides the achievement in displacement measurements fusion, challenges are also present. Even though rapid development has been obtained in the recent years, the fusion of heterogeneous measurements, from SAR, optical images, GPS and other sources of information, still remains a delicate problem. No fusion method nor strategy is completely operational to deal with diverse characteristics and **uncertainty** levels

of the heterogeneous measurements in an inversion system. No efficient solution has been proposed to the determination of the contribution of each individual measurement, as well as their covariance. From the computational point of view, even with the availability of supercomputing facilities, we can still be quickly limited by the memory and storage capacity, as well as the computation time, given the high spatial resolution and the strong repetitiveness of acquisitions. For **accuracy** and uncertainty consideration, **on one hand, the quantification and the improvement of the accuracy are always very challenging, given that in most cases the ground truth is not available. On the other hand,** it is always difficult to characterise the uncertainty in displacement measurements, then to choose an appropriate uncertainty management approach. In satellite imagery, uncertainty comes from different perturbations generated along the wave propagation path, at the back-scattering surface, as well as from noise generated in the electronic processing. In addition, imperfect corrections (atmospheric and/or geometric corrections) performed in the displacement extraction chain also introduce systematic uncertainties. These diverse sources result in uncertainties of complex characteristics. Moreover, in case of model inversion, it is very difficult to propagate the uncertainty. The retrieved deformation models are often provided without uncertainty information. The evaluation of these models obtained with more or less different measurements is thus a challenging task. For example, in the case of the Kashmir earthquake (2005), [12, 32, 117, 34] obtained different fault rupture models by using different surface displacement measurements. Without ground truth, it is impossible to assess these models in an objective way.

Given the current status and the future development of displacement measurement fusion, **sophisticated statistic tools, such as the Kalman Filter, the Bayesian theory and so on, can be expected to further improve the results. Meanwhile,** it will be important to modify the processing algorithms and to adapt our way of working. Inspired from the ocean reanalysis, different measurements with different spatial coverage, different spatial resolution, different time spans, bringing different information, including correlation of SAR, optical images, DInSAR, GPS and other in situ measurements, can be homogenised through a realistic physical model in order to produce spatially and temporally regular displacement maps (namely displacement reanalysis) to record the properties of the displacement over time. Later, instead of keeping and processing different types of measurements of large volume, these displacement reanalyses present numerous advantages. Currently, the displacement measurement by remote sensing is still mainly applied to past events that have taken place before the data processing. With the launching by ESA of the Sentinel series, remote sensing data can be acquired nearly everywhere on the Earth at least every 6 days. By adding the data issued from other satellites, TerraSAR-X and TanDEM-X, Landsat 8, the four satellites **COSMO-SkyMed**, ALOS-2, etc, real time monitoring by time series will

become possible. The combination in real time of displacement measurements from remote sensing imagery and physical models is possible. It will thus be possible to predict the evolution of an event such as a magma reload of a reservoir located beneath an active volcano or a rupture of a serac. Data assimilation extensively investigated in atmosphere and ocean science will open new perspective for the observation and the prevention of natural hazards.

References

[1] J. Anhorn and B. Khazai, "Open space suitability analysis for emergency shelter after an earthquake," *Natural Hazards and Earth System Science*, vol. 15, pp. 789–803, 2015.

[2] W. T. Yang, M. Wang, N. Kerle, C. J. V. Westen, L. Y. Liu, and P. J. Shi, "Analysis of changes in post-seismic landslide distribution and its effect on building reconstruction," *Natural Hazards and Earth System Science*, vol. 15, pp. 817–825, 2015.

[3] B. Fruneau, J. Achache, and C. Delacourt, "Observation and modelling of the Saint-Etienne-de-Tinée landslide using SAR interferometry," *Tectonophysics*, vol. 265, pp. 181–190, 1996.

[4] T. Wang, D. Perissin, F. Rocca, and M. Liao, "Three Gorges Dam stability monitoring with time-series InSAR image analysis," *Science China Earth Sciences*, vol. 54, no. 5, pp. 720–732, 2011.

[5] G. Vasile, A. Anghel, D. Boldo, R. Boudon, G. D'Urso, and R. Muja, "Potential of multi-pass high-resolution SAR interferometry for dam monitoring," *MTA Review*, vol. 22, no. 4, pp. 235–246, 2012.

[6] J. Sousa and L. Bastos, "Multi-temporal sar interferometry reveals acceleration of bridge sinking before collapse," *Natural Hazards and Earth System Science*, vol. 13, pp. 659–667, 2013.

[7] P. Lopez-Quiroz, M. P. Doin, F. Tupin, P. Briole, and J. M. Nicolas, "Time series analysis of Mexico City subsidence constrained by radar interferometry," *Journal of Applied Geophysics*, vol. 69, no. 1, pp. 1–15, 2009.

[8] Q. Luo, D. Perissin, H. Lin, Y. Zhang, and W. Wang, "Subsidence Monitoring of Tianjin Suburbs by TerraSAR-X Persistent Scatterers Interferometry," *IEEE Transactions on Geoscience and Remote Sensing*, vol. 7, no. 5, pp. 1642–1650, 2014.

[9] K. Goel and N. Adam, "A Distributed Scatterer Interferometry Approach for Precision Monitoring of Known Surface Deformation Phenomena," *IEEE Transactions on Geoscience and Remote Sensing*, vol. 52, no. 9, pp. 5454–5468, 2014.

[10] R. Iglesias, A. Aguasca, X. F. J. Mallorqui, D. Monells, C. C. Lopez-Martinez, and L. Pipia, "Ground-Based Polarimetric SAR Interferometry for the Monitoring of Terrain Displacement Phenomena–Part I: Theoretical Description," *IEEE Journal of Selected Topics in Applied Earth Observations and Remote Sensing*, vol. 8, no. 3, pp. 980 – 993, 2015.

[11] R. Iglesias, A. Aguasca, X. F. J. Mallorqui, D. Monells, C. C. Lopez-Martinez, and L. Pipia, "Ground-Based Polarimetric SAR Interferometry for the Monitoring of Terrain Displacement Phenomena–Part II: Applications," *IEEE Journal of Selected Topics in Applied Earth Observations and Remote Sensing*, vol. 8, no. 3, pp. 994 – 1007, 2015.

[12] E. Pathier, E. J. Fielding, T. J. Wright, R. Walker, B. E. Parsons, and S. Hensley, "Displacement field and slip distribution of the 2005 Kashmir earthquake from SAR imagery," *Geophysical Research Letters*, vol. 33, no. L20310, pp. 1–5, 2006.

[13] N. D'Agostino, D. Cheloni, G. Fornaro, R. Giuliani, and D. Reale, "Space-time distribution of after-slip following the 2009 L'Aquila earthquake," *Journal of Geophysical Research*, vol. 117, no. B02402, pp. 1–23, 2012.

[14] R. Jolivet, C. Lasserre, M. Doin, G. Peltzer, J. Avouac, R. Dailu, and J. Sun, "Spatio-temporal evolution of aseismic slip along the haiyuan fault, china : Implications for fault frictional properties," *Earth and Planetary Science Letters*, vol. 377-378, pp. 22–33, 2013.

[15] D. Cheloni, R. Giuliani, E.D'Anostasio, S. Atzori, R. Walters, L. Bonci, N. D'Agostino, M. Mattone, S. Calcaterra, P. Gambino, F. Deninno, R. Maseroli, and G. Stefanelli, "Coseismic and post-seismic slip of the 2009 L'Aquila (central Italy) Mw 6.3 earthquake and implications for seismic potential along the Campotosto fault from joint inversion of high-precision levelling, Insar and GPS data," *Tectonophysics*, vol. 622, pp. 168–185, 2014.

[16] D. Bekaert, A. Hooper, and T. Wright, "Reassessing the 2006 Guerrero slow-slip event, Mexico: Implications for large earthquakes in the Guerrero Gap," *Journal of Geophysical Research*, vol. 120, no. 2, pp. 1357–1375, 2015.

[17] E. Berthier, H. Vadon, D. Baratous, Y. Arnaud, C. Vincent, K. L. Feigl, F. Rémy, and B. Legrésy, "Surface motion of mountain glaciers derived from satellite optical imagery," *Remote Sensing of Environment*, vol. 95, pp. 14–28, 2006.

[18] E. Rignot, J. Mouginot, and B. Scheuchl, "Ice flow of the Antarctic ice sheet," *Science*, vol. 333, pp. 1427–1430, 2011.

[19] A. Dehecq, N. Gourmelen, and E. Trouvé, "Deriving large-scale glacier velocities from a complete satellite archive : Application to the Pamir-Karakoram-Himalaya," *Remote Sensing of Environment*, vol. 162, pp. 55–66, 2015.

[20] F. Sigmundsson, S. Hreinsdottir, A. Hooper, T. Arnadottir, R. Pedersen, M. J. Roberts, N. Oskarsson, A. Auriac, J. Decriem, P. Einarsson, H. Geirsson, M. Hensch, B. Ofeigsson, E. Sturkell, H. Sveinbjornsson, and K. L. Feigl, "Intrusion triggering of the 2010 Eyjafjallajökull explosive eruption," *Nature*, vol. 468, pp. 426–430, 2010.

[21] A. Hooper, F. Prata, and F. Sigmundsson, "Remote sensing of Volcanic Hazards and Their Precursors," *Proceedings of the IEEE*, vol. 100, pp. 2908–2930, 2012.

[22] A. Auriac, K. Spaans, F. Sigmundsson, A. Hooper, P. Schmidt, and B. Lund, "Iceland rising: Solid Earth response to ice retreat inferred from satellite radar interferometry and visocelastic modeling," *Journal of Geophysical Research*, vol. 118, no. 4, pp. 1331–1344, 2013.

[23] V. Pinel, M. Poland, and A. Hooper, "Volcanology: Lessons learned from Synthetic Aperture Radar imagery," *Journal of Volcanology and Geothermal Research*, vol. 289, pp. 81–113, 2014.

[24] R. Michel, J. Avouac, and J. Taboury, "Measuring ground displacements from sar amplitude images: application to the landers earthquake," *Geophysical Research Letters*, vol. 26, no. 7, pp. 875–878, 1999.

[25] M. Tobita, M. Murakami, H. Nakagawa, and H. Yarai, "3-D surface deformation of the 2000 Usu eruption measured by matching of SAR images," *Geophysical Research Letters*, vol. 28, no. 22, pp. 4291–4294, 2001.

[26] F. Casu, A. Manconi, A. Pepe, and R. Lanari, "Deformation Time-Series Generation in Areas Characterized by Large Displacement Dynamics: The SAR Amplitude Pixel-Offset SBAS Technique," *IEEE Transactions on Geoscience and Remote Sensing*, vol. 49, no. 99, pp. 1–12, 2011.

[27] S. Leprince, S. Barbot, F. Ayoub, and J. Avouac, "Automatic and Precise Orthorectification, Coregistration, and Subpixel Correlation of Satellite Images, Application to Ground Deformation Measurements," *IEEE Transactions on Geoscience and Remote Sensing*, vol. 45, no. 6, pp. 1529–1558, 2007.

[28] T. Scambos, M. Dutkiewicz, J. Wilson, and R. Bindshadler, "Application of image cross-correlation to the measurement of glacier velocity using satellite image data," *Remote Sensing of Environment*, vol. 42, pp. 177–186, 1992.

[29] E. Berthier, H. Vadon, D. Baratoux, Y. Arnaud, C. Vincent, K. Feigl, F. Remi, and B. Legresy, "Surface motion of mountain glaciers derived from satellite optical imagery," *Remote Sensing of Environment*, vol. 95, pp. 14–28, 2005.

[30] A. Luckman, D. Quincey, and S. Bevan, "The potential of satellite radar interferometry and feature tracking for monitoring flow rates of himalayan glaciers," *Remote Sensing of Environment*, vol. 111, pp. 172–181, 2007.

[31] F. Vernier, R. Fallourd, J. M. Friedt, Y. Yan, E. Trouvé, J. Nicolas, and L. Moreau, "Fast Correlation Technique for Glacier Flow Monitoring by Digital Camera and Space-borne SAR Images," *EURASIP Journal on Image and Video Processing*, 2011.

[32] J. Avouac, F. Ayoub, S. Leprince, O. Konca, and D. V. Helmberger, "The 2005, $M_w7.6$ Kashmir earthquake: Sub-pixel correlation of ASTER images and seismic waveforms analysis," *Earth and Planetary Science Letters*, vol. 249, no. 3-4, pp. 514–528, 2006.

[33] Z. Li, J. Elliott, W. Feng, J. Jackson, B. Parsons, and R. Walters, "The 2010 Mw 6.8 Yushu (Qinghai, China) earthquake: Constraints provided by InSAR and body wave seismology," *Journal of Geophysical Research*, vol. 116, no. B10302, pp. 1–16, 2011.

[34] Y. Yan, V. Pinel, E. Trouvé, E. Pathier, J. Perrin, P. Bascou, and F. Jouanne, "Coseismic displacement field and slip distribution of the 2005 kashmir earthquake from SAR amplitude image correlation and differential interferometry," *Geophysical Journal International*, vol. 193, no. 1, pp. 29–46, 2013.

[35] X. Hu, T. Wang, and M. Liao, "Measuring coseismic displacements with point-like targets offset tracking," *IEEE Geoscience and Remote Sensing Letters*, vol. 11, no. 1, pp. 283–287, 2014.

[36] G. Liu, H. Jia, R. Zhang, H. Zhang, H. Jia, B. Yu, and M. Sang, "Exploration of Subsidence Estimation by Persistent Scatterer InSAR on Time Series of High Resolution TerraSAR-X Images,"

IEEE Journal of Selected Topics in Applied Earth Observations and Remote Sensing, vol. 4, no. 1, pp. 159 – 170, 2011.

[37] R. Zhang, G. Liu, T. Li, L. Huang, B. Yu, Q. Chen, and Z. Li, "An Integrated Model for Extracting Surface Deformation Components by PSI Time Series," *IEEE Geoscience and Remote Sensing Letters*, vol. 11, no. 2, pp. 544 – 548, 2014.

[38] O. Cavalié, E. Pathier, M. Radiguet, M. Vergnolle, N. Cotte, A. Walpersdorf, V. Kostoglodov, and F. Cotton, "Slow slip event in the mexican subduction zone: Evidence of shallower slip in the guerrero seismic gap for the 2006 event revealed by the joint inversion of InSAR and GPS data," *Earth and Planetary Science Letters*, vol. 367, pp. 52–60, 2013.

[39] R. Goldstein, H. Englehardt, B. Kamb, and R. Frolich, "Satellite radar interferometry for monitoring ice sheet motion : application to an Antarctic Ice Stream," *Science*, vol. 262, no. 1, pp. 525–530, 1993.

[40] J. Mohr, N. Reeh, and S. Madsen, "Three-dimensional glacial flow and surface elevation measured with radar interferometry," *Nature*, vol. 391, pp. 273–276, 1998.

[41] E. Trouvé, G. Vasile, M. Gay, L. Bombrun, P. Grussenmeyer, T. Landes, J. Nicolas, P. Bolon, I. Petillot, and A. Julea, "Combining airborne photographs and spaceborne sar data to monitor temperate glaciers: Potentials and limits," *IEEE Transactions on Geoscience and Remote Sensing, IEEE Transactions*, vol. 45, pp. 905–924, 2007.

[42] A. Ferretti, C. Prati, and F. Rocca, "Permanent scatterer in SAR interferometry," *IEEE Transactions on Geoscience and Remote Sensing*, vol. 39, no. 1, pp. 8–20, 2001.

[43] C. Werner, U. Wegmuller, T. Strozzi, and A.Wiesmann, "Interferometric point target analysis for deformation mapping," in *Geoscience and Remote Sensing Symposium*, vol. 7, pp. 4362–4364, 2003.

[44] B. M. Kampes, *Radar interferometry : persistent scatterer technique.* Springer, 2006.

[45] A. Hooper, P. Segall, and H. Zebker, "Persistent scatterer interferometric synthetic aperture radar for crustal deformation analysis with application to Volcan Alcedo, Galapagos," *Journal of Geophysical Research*, vol. 112, no. B07407, 2007.

[46] P. Rosen, I. J. S. Hensley, F. Li, S. Madsen, E. Rodriguez, and R. Goldstein, "Synthetic aperture radar interferometry," *Proceedings of the IEEE*, vol. 88, no. 3, pp. 333–382, 2000.

[47] P. Berardino, G. Fornaro, R. Lanari, and E. Santosti, "A new algorithm for surface deformation monitoring based on small baseline differential sar interferograms," *IEEE Transactions on Geoscience and Remote Sensing*, vol. 40, no. 11, pp. 2375–2383, 2002.

[48] D. A. Schmidt and R. Bürgmann, "Time-dependent land uplift and subsidence in the santa clara valley, california, from a large interferometric synthetic aperture radar data set," *Journal of Geophysical Research*, vol. 108, no. B9, pp. ETG4.1–ETG4.13, 2003.

[49] S. Usai, "A least squares database approach for sar interferometric data," *IEEE Transactions on Geoscience and Remote Sensing*, vol. 41, no. 4, pp. 753–760, 2003.

[50] R. Lanari, O. Mora, M. Manunta, J. Mallorqui, P. Berardino, and E. Sansosti, "A Small-Baseline Approach for Investigating Deformations on Full-Resolution Differential SAR Interferograms," *IEEE Transaction on Geoscience and Remote Sensing*, vol. 42, no. 7, pp. 1377–1386, 2004.

[51] Y. Yan, M. P. Doin, P. Lopez-Quiroz, F. Tupin, B. Fruneau, V. Pinel, and E. Trouvé, "Mexico city subsidence measured by Insar time series: Joint analysis using PS and SBAS approaches," *IEEE Journal of Selected Topics in Applied Earth Observations and Remote Sensing*, vol. 5, no. 4, pp. 1312–1326, 2012.

[52] G. Liu, H. Jia, Y. Nie, T. Li, R. Zhang, and B. Yu, "Detecting subsidence in coastal areas by ultrashort baseline TCPInSAR on time series of high resolution TerraSAR-X images," *IEEE Transactions on Geoscience and Remote Sensing*, 2013.

[53] S, "Measuring two-dimensional movements using a single InSAR pair," *Geophysical Research Letter*, vol. 33, no. L16311, pp. 1–5, 2006.

[54] H. Jung, S. Yun, and M. Jo, "An Improvement of Multiple-Aperture SAR Interferometry Performance in the Presence of Complex and Large Line-of-Sight Deformation," *IEEE Journal of Selected Topics in Applied Earth Observations and Remote Sensing*, vol. 8, no. 4, pp. 1743 – 1752, 2015.

[55] O. Monserrat, M. Crosetto, M. Cuevas, and B. Crippa, "The thermal expansion component of Persistent Scatterer Interferometry observations," *IEEE GEOSCIENCE AND REMOTE SENSING LETTERS*, vol. 8, no. 5, pp. 864 – 868, 2011.

[56] G. Fornaro, D. Reale, and S. Verde, "Bridge thermal dilation monitoring with millimeter sensitivity via multidimensional SAR imaging," *IEEE GEOSCIENCE AND REMOTE SENSING LETTERS*, vol. 10, no. 4, pp. 677 – 681, 2010.

[57] D. Reale, G. Fornaro, and A. Pauciullo, "Extension of 4-D SAR imaging to the monitoring of thermally dilating scatterers," *IEEE Transactions on Geoscience and Remote Sensing*, vol. 51, no. 12, pp. 5296–5306, 2013.

[58] H. Matsuda and N. Shimizu, "Assessment of rock slope stability based on the three-dimensional continuous displacement monitoring by Global Positioning System," *International Journal of the JCRM*, vol. 2, no. 1, pp. 17–20, 2006.

[59] F. Jouanne, A. Awan, A. Madji, A. Pêcher, M. Latif, A. Kausar, J. Mugnier, I. Khan, and N. Khan, "Post-seismic deformation in Pakistan after the October 8, 2005 earthquake: evidence of afterslip along a flat north of the Balakot-Bagh trust," *Journal of Geophysical Research*, vol. 116, no. B07401, 2011.

[60] T. Reverso, J. Vandemeulebrouck, F. Jouanne, V. Pinel, T. Villemin, E. Sturkell, and P. Bascou, "A two-magma chamber model as a source of deformation at grímsvötn volcano, Iceland," *Journal of Geophysical Research*, vol. 119, pp. 4666–4683, 2014.

[61] F. Ponton, E. Trouvé, M. Gay, A. Walpersdorf, R. Fallourd, J. Nicolas, F. Vernier, and J. Mugnier, "Observation of the argentière glacier flow variability from 2009 to 2011 by TerraSAR-X and GPS displacement measurements," *Journal of Selected Topics in Applied Earth Observations and Remote Sensing*, vol. 7, no. 8, 2014.

[62] E. Calais, J. Han, C. DeMets, and J. Noquet, "Deformation of the North American plate interior from a decade of continuous GPS measurements," *Journal of Geophysical Research*, vol. 111, no. B06402, pp. 1–23, 2006.

[63] P. Capuano, G. D. Natale, P. Gasparini, F. Pingue, and R. Scarpa, "A model for the 1908 Messina Straits (Italy) earthquake by inversion of levelling data," *Bulletin of the Seismological Society of America*, vol. 78, no. 6, pp. 1930 – 1947, 1988.

[64] R. Bürgmann, P. Segall, M. Lisowski, and J. Svarc, "Postseismic strain following the 1989 Loma Prieta earthquake from GPS and leveling measurements," *Journal of Geophysical Research*, vol. 102, no. B3, pp. 4933 – 4955, 1997.

[65] M. Motagh, Y. Djamour, T. Walter, H. Wetzel, J. Zschau, and S. Arabi, "Land subsidence in Mashhad Valley, northeast Iran: Results from InSAR, levelling and GPS," *Geophysical Journal International*, vol. 168, no. 2, pp. 518–526, 2007.

[66] K. Chen, M. Yang, Y. Huang, K. Ching, and R. Rau, "Vertical displacement rate field of taiwan from geodetic levelling data 2000-2008," *Survey Review*, vol. 43, no. 321, pp. 296–302, 2011.

[67] R. Fallourd, O. Harant, E. Trouvé, J. M. Nicolas, M. Gay, A. Walpersdorf, J. L. Mugnier, J. Serafini, D. Rosu, L. Bombrun, G. Vasile, N. Cotte, F. Vernier, F. Tupin, L. Moreau, and P. Bolon, "Monitoring Temperate Glacier Displacement by Multi-Temporal TerraSAR-X Images and Continuous GPS Measurements," *IEEE Journal of Selected Topics in Applied Earth Observations and Remote Sensing*, vol. 4, no. 2, pp. 372–386, 2011.

[68] E. Burgess, R. Forster, and C. Larsen, "Flow velocities of alaskan glaciers," *Nature communications*, vol. 4, 2013.

[69] O. Cavalié, M. P. Doin, C. Lasserre, and P. Briole, "Ground motion measurement in the lake Mead area, Nevada, by differential synthetic aperture radar interferometry time series analysis: Probing the lithosphere rheological structure," *Journal of Geophysical Research*, vol. 112, no. B03403, 2007.

[70] E. Trouvé, J. M. Nicolas, and H. Maitre, "Improving Phase Unwrapping Techniques by the Use of Local Frequency Estimates," *IEEE Transaction on Geoscience and Remote Sensing*, vol. 36, no. 6, pp. 1963–1972, 1998.

[71] R. B. Lohman and M. Simons, "Some thoughts on the use of InSAR data to constain models of surface deformation: Noise structure and data downsampling," *Geochemistry, Geophysics, Geosystems*, vol. 6, no. 1, pp. Q01007.1–Q01007.12, 2005.

[72] H. Sudhaus and S. Jónsson, "Improved source modelling through combined use of InSAR and GPS under consideration of correlated data errors: application to the June 2000 Kleifarvatn earthquake, Iceland," *Geophysical Journal International*, vol. 176, no. 2, pp. 389–404, 2009.

[73] J. Zhang, Y. Bock, H. Johnson, P. Fang, S. Williams, J. Genrich, S. Wdowinski, and J. Behr, "Southern California Permanent GPS Geodetic Array: Error analysis of daily position estimates and site velocities," *Journal of Geophysical Research*, vol. 102, no. B8, pp. 18035–18055, 1997.

[74] T. Arnadottir, P. Segall, and M. Matthews, "Resolving the discrepancy between geodetic and seismic fault models for the 1989 Loma Prieta, California, earthquake," *Bulletin of the Seismological Society of America*, vol. 82, no. 5, pp. 2248 – 2255, 1992.

[75] A. Amoruso and L. Crescentini, "Inversion of levelling data: how important is error treatment?," *Geophysical Journal International*, vol. 171, no. 3, pp. 1352–1362, 2007.

[76] T. Wright, B. Parsons, and E. Fielding, "Measurement of interseismic strain accumulation across the north anatolian fault by satellite radar interferometry," *Geophysical Research Letters*, vol. 28, no. 10, pp. 2117–2120, 2001.

[77] S. Lyons and D. Sandwell, "Fault creep along the southern san andreas from interferometric synthetic aperture radar, permanent scatterers, and stacking," *Journal of Geophysical Research*, vol. 108, no. B1, 2003.

[78] D. A. Schmidt, R. Bürgmann, R. M. Nadeau, and M. d'Alessio, "Distribution of aseismic slip rate on the Hayward fault inferred from seismic and geodetic data," *Journal of Geophysical Research*, vol. 110, no. B08406, pp. 1–15, 2005.

[79] O. Cavalié, C. Lasserre, M.-P. Doin, G. Peltzer, J. Sun, X. Xu, and Z.-K. Shen, "Measurement of interseismic strain across the Haiyuan fault (Gansu, China), by InSAR," *Journal of Geophysical Research*, vol. 275, no. 3-4, pp. 246 – 257, 2008.

[80] A. Hooper, H. Zebker, P. Segall, and B. Kampes, "A new method for measuring deformation on volcanoes and other natural terrains using InSAR persistent scatterers," *Geophysical Research Letters*, vol. 31, 2004.

[81] F. Casu, S. Elefante, P. Imperatore, I. Zinno, M. Manunta, C. D. Luca, and R. Lanari, "Sbas-dinsar Parallel Processing for Deformation Time-Series Computation," *IEEE Journal of Selected Topics in Applied Earth Observations and Remote Sensing*, vol. 7, no. 8, pp. 3285–3296, 2014.

[82] A. Ferretti, A. Fumagalli, F. Novali, C. Prati, F. Rocca, and A. Rucci, "A New Algorithm for Processing Interferometric Data-Stacks: SqueeSAR," *IEEE Transactions on Geoscience and Remote Sensing*, vol. 49, no. 9, pp. 3460–3470, 2011.

[83] F. Lombardini, "Differential tomography:anewframework forsarinterferometry," *IEEE Transactions on Geoscience and Remote Sensing*, vol. 43, no. 1, pp. 37–44, 2005.

[84] G. Fornaro, D. Reale, and F. Serafino, "Four-dimensional SAR imaging for height estimation and monitoring of single and double scatterers," *IEEE Transactions on Geoscience and Remote Sensing*, vol. 47, no. 1, pp. 224–237, 2009.

[85] G. Fornaro, F. Serafino, and D. Reale, "4D SAR imaging: The case study of Rome," *IEEE GEOSCIENCE AND REMOTE SENSING LETTERS*, vol. 7, no. 2, pp. 236 – 240, 2010.

[86] X. Zhu and R. Bamler, "Very high resolution spaceborne SAR tomography in urban environment," *IEEE Transactions on Geoscience and Remote Sensing*, vol. 48, no. 12, pp. 4296–4308, 2010.

[87] D. Reale, G. Fornaro, A. Pauciullo, X. Zhu, and R. Bamler, "Tomographic imaging and monitoring of buildings with very high resolution SAR data," *IEEE GEOSCIENCE AND REMOTE SENSING LETTERS*, vol. 8, no. 4, pp. 661 – 665, 2011.

[88] Y. Fialko, M. Simons, and D. Agnew, "The complete (3-D) surface displacement field in the epicentral area of the 1999 Mw 7.1 Hector Mine earthquake, California, from space geodetic observations," *Geophysical Research Letters*, vol. 28, no. 16, p. 3063–3066, 2001.

[89] T. J. Wright, B. E. Parsons, and Z. Lu, "Toward mapping surface deformation in three dimensions using InSAR," *Geophysical Research Letters*, vol. 31, no. L01607, pp. 1–5, 2004.

[90] T. Wang and S. Jonsson, "Improved SAR amplitude image offset measurements for deriving three-dimensional coseismic displacements," *IEEE Journal of Selected Topics in Applied Earth Observations and Remote Sensing*, vol. 8, no. 7, pp. 3271 – 3278, 2015.

[91] D. Dubois and H. Prade, *Possibility theory: An Approach to Computerized Processing of Uncertainty*. Plenum Press, 1988.

[92] D. Dubois, L. Foulloy, G. Mauris, and H. Prade, "Probability-possibility transformations, triangular fuzzy sets and probabilistic inequalities," *International Journal on Reliable Computing*, vol. 10, no. 4, pp. 273–297, 2004.

[93] L. A. Zadeh, "Fuzzy sets as a basis for a theory of possibility," *Fuzzy Sets and Systems*, vol. 1, no. 1, pp. 3–28, 1978.

[94] Y. Yan, E. Trouvé, V. Pinel, G. Mauris, E. Pathier, and S. Galichet, "Fusion of D-InSAR and sub-pixel image correlation measurements for coseismic displacement field estimation: Application to the Kashmir earthquake (2005)," *International Journal of Image and Data Fusion*, vol. 3, no. 1, pp. 71–92, 2012.

[95] Y. Okada, "Surface deformation due to shear and tensile faults in a half-space," *Bulletin of the Seismological Society of America*, vol. 75, no. 4, pp. 1135–1154, 1985.

[96] K. Mogi, "Relations between the Eruptions of Various Volcanoes and the Deformations of the Ground Surfaces around them," *Bulletin of the Earthquake Research Institute*, vol. 36, pp. 99–134, 1958.

[97] M. Simons, Y. Fialko, and L. Rivera, "Coseismic deformation from the 1999 m_w 7.1 Hector Mine, California, Earthquake as Inferred from InSAR and GPS observations," *Bulletin of the Seismological Society of America*, vol. 92, no. 4, pp. 1390–1402, 2002.

[98] S. Jónsson, H. Zebker, P. Segall, and F. Amelung, "Fault Slip Distribution of the 1999 M_w7.1 Hector Mine, California, Earthquake, Estimated from Satellite Radar and GPS Measurements," *Bulletin of the Seismological Society of America*, vol. 92, no. 4, pp. 1377–1389, 2002.

[99] R. Pedersen, S. Jónsson, T. Arnadóttir, F. Sigmundsson, and K. L. Feigl, "Fault slip distribution of two June 2000 M_w6.5 earthquake in South Iceland estimated from joint inversion of InSAR and GPS measurements," *Earth and Planetary Science Letters*, vol. 213, no. 3-4, pp. 487–502, 2003.

[100] G. J. Funning, B. Parsons, and T. J. Wright, "Surface displacements and source parameters of the 2003 Bam (Iran) earthquake from Envisat advanced synthetic aperture radar imagery," *Journal of Geophysical Research*, vol. 110, no. B09406, pp. 1–23, 2005.

[101] S. Wei, E. Fielding, S. Leprince, A. Sladen, J. Avouac, D. Helmberger, E. Hauksson, R. Chu, M. Simons, K. Hudnut, T. Herring, and R. Briggs, "Superficial simplicity of the 2010 Elmayor–Cucapah earthquake of Baja California in Mexico," *Nature Geoscience*, vol. 4, pp. 615 –618, 2011.

[102] J. Beavan, E. Fielding, M. Motagh, S. Samsonov, and N. Donnelly, "Fault location and slip distribution of the 22 February 2011 Mw 6.2 Christchurch, New Zealand, earthquake from geodetic data," *Seismological Research Letters*, vol. 82, no. 6, pp. 789 – 799, 2011.

[103] E. Fielding, M. Simons, S. Owen, P. Lundgren, H. Hua, P. Agram, Z. Liu, A. Moore, P. Milillo, J. Polet, S. Samsonov, P. Rosen, F. Webb, and G. Milillo, "Rapid imaging of earthquake ruptures with combined geodetic and seismic analysis," *Procedia Technology*, vol. 16, pp. 876 – 885, 2014.

[104] W. Barnhart, J. R. Murray, S.-H. Yun, J. L. Svarc, S. V. Samsonov, E. J. Fielding, B. A. Brooks, and P. Milillo, "Geodetic constraints on the 2014 M 6.0 South Napa earthquake," *Seismological Research Letters*, vol. 86, no. 2A, pp. 335 –343, 2015.

[105] Y. Fialko, "Interseismic strain accumulation and the earthquake potential on the southern San Andreas fault system," *Nature*, vol. 441, pp. 968–971, 2006.

[106] D. Massonnet, K. Feigl, M. Rossi, and F. Adragna, "Radar interferometric mapping of deformation in the year after the Landers earthquake," *Nature*, vol. 369, pp. 227–230, 1994.

[107] Y. Fialko, "Evidence of fluid-filled upper crust from observations of postseismic deformation due to the 1992 Mw7. 3 Landers earthquake," *Journal of Geophysical Research*, vol. 109, no. B08401, pp. 1–17, 2004.

[108] L. Bruhat, S. Barbot, and J. Avouac, "Evidence for postseismic deformation of the lower crust following the 2004 Mw6.0 parkfield earthquake," *Journal of Geophysical Research*, vol. 116, no. B08401, pp. 1–10, 2011.

[109] D. Sandwell, D. Myer, R. Mellors, and M. Shimada, "Accuracy and resolution of ALOS interferometry: vector deformation maps of the father's day intrusion at Kilauea," *IEEE Transactions on Geoscience and Remote Sensing*, vol. 46, no. 11, pp. 3524–3534, 2008.

[110] G. Evensen, "The Ensemble Kalman Filter: theoretical formulation and practical implementaion," *Ocean Dynamics*, vol. 53, pp. 343–367, 2003.

[111] Y. Yan, E. Trouvé, and V. Pinel, "Fusion of prior information and multi-scales local frequencies to facilitate D-InSAR phase unwrapping," in *IEEE International Symposium on Geoscience and Remote Sensing*, (Munich), pp. 1888–1891, 2012.

[112] S. Yun, H. Zebker, P. Segall, A. Hooper, and M. Poland, "Interferogram formation in the presence of complex and large deformation," *Geophysical Research Letter*, vol. 34, no. L12305, pp. 1–6, 2007.

[113] S. Atzori, I. Hunstad, M. Chini, S. Salvi, C. Tolomei, C. Bignami, S. Stramondo, E. Trasatti, A. Antonioli, and E. Boschi, "Finite fault inversion of DInSAR coseismic displacement of the 2009 L'Aquila earthquake (central Italy)," *Geophysical Research Letter*, vol. 36, no. L15305, pp. 1–6, 2009.

[114] K. L. Feigl and C. H. Thurber, "A method for modelling radar interferograms without phase unwrapping: application to the M 5 Fawnskin, California earthquake of 1992 December 4," *Geophysical Journal International*, vol. 176, no. 2, pp. 491–504, 2009.

[115] G. Fornaro, S. Atzori, F. Calò, D. Reale, and S. Salvi, "Inversion of wrapped differential interferometric SAR data for fault dislocation modeling," *IEEE Transactions on Geoscience and Remote Sensing*, vol. 50, no. 6, pp. 2175 – 2184, 2012.

[116] D. Baù, M. Ferronato, G. Gambolati, P. Teatini, and A. Alzraiee, "Ensemble smoothing of land subsidence measurements for reservoir geomechanical characterization," *INTERNATIONAL JOURNAL FOR NUMERICAL AND ANALYTICAL METHODS IN GEOMECHANICS*, vol. 39, no. 2, pp. 207–228, 2015.

[117] H. Wang, L. Ge, C. Xu, and Z. Du, "3-d coseismic displacement field of the 2005 Kashmir earthquake inferred from satellite radar imagery," *Earth Planets Space*, vol. 59, no. 5, pp. 343 – 349, 2007.

[118] A. Manconi and F. Casu, "Joint analysis of displacement time series retrieved from SAR phase and amplitude: Impact on the estimation of volcanic source parameters," *Geophysical Research Letters*, vol. 39, no. 14, 2012.
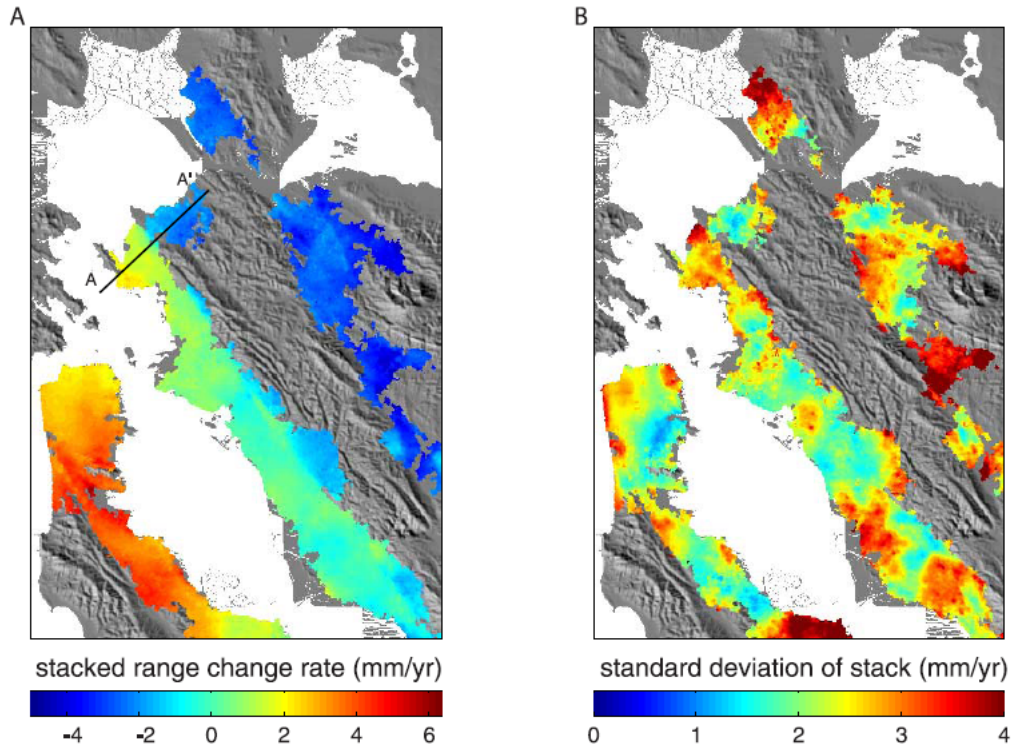
List of Figures

Figure 1: (a) Linear range change rate (b) standard deviation of the linear range change rate obtained from stacking of 13 independent interferograms in the San Francisco Bay Area from 1992 to 2000 (from [78]).
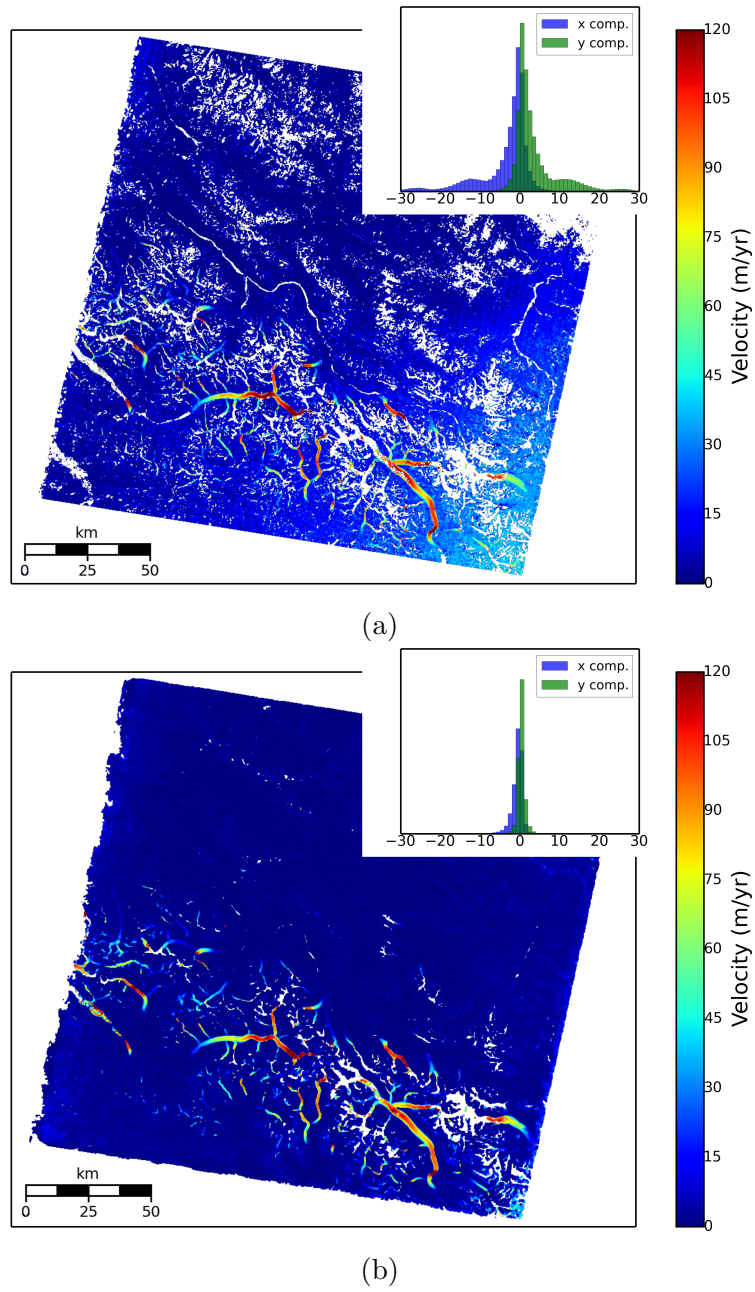
Figure 2: Ice flow velocity magnitude obtained from feature-tracking of Landsat images over the Karakoram for (a) a single annual pair (b) the fusion of 29 annual pairs over the period 1999-2001. White gaps correspond to areas where no measurements are available. In (a) the spatial coverage is 70%, while it is increased to 94% in (b). Insets show histograms of the velocity in stable areas for each component.
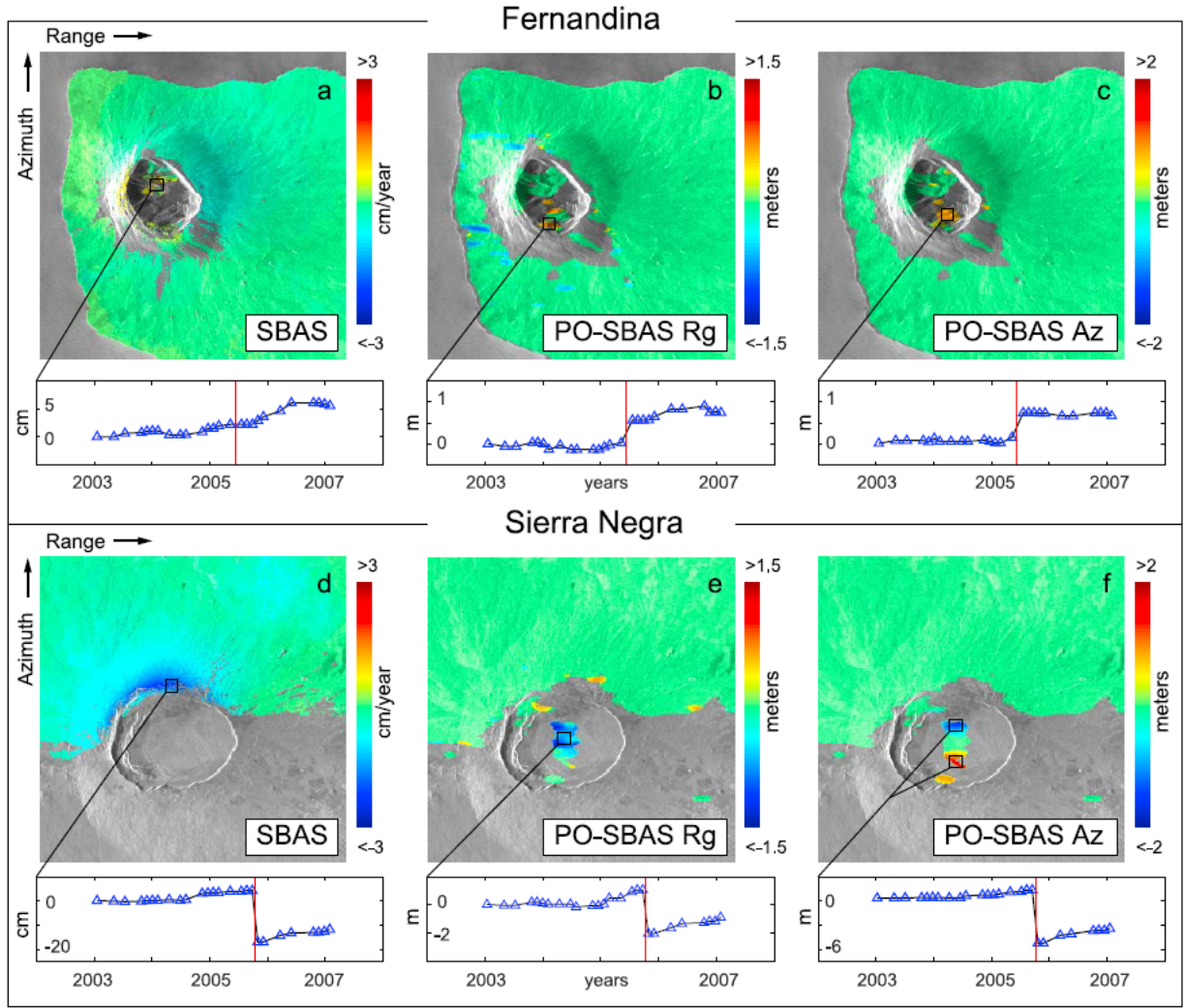
Figure 3: Example of displacement time series obtained with SBAS and P0-SBAS for Fernandina (a-c) and Sierra Negra (d-f) (from [118]). (a) LOS mean deformation velocity map computed through the SBAS approach and the displacement time series relevant to a point located in the inner caldera denoted by the black square (b-c) Displacement during the period of 2003 - 2007 computed through the PO-SBAS approach along the range and the azimuth directions and the displacement time series of representative points located within the inner caldera. (d) Same as (a) but for Sierra Negra (e) Same as (b) but for Sierra Negra (f) Same as (c) but for Sierra Negra. The displacement time series is relevant to the relative displacement between two points located across the caldera, identified by the black boxes. Red lines refer to the Fernandina May 2005 eruption and to the Sierra Negra October 2005 eruption.
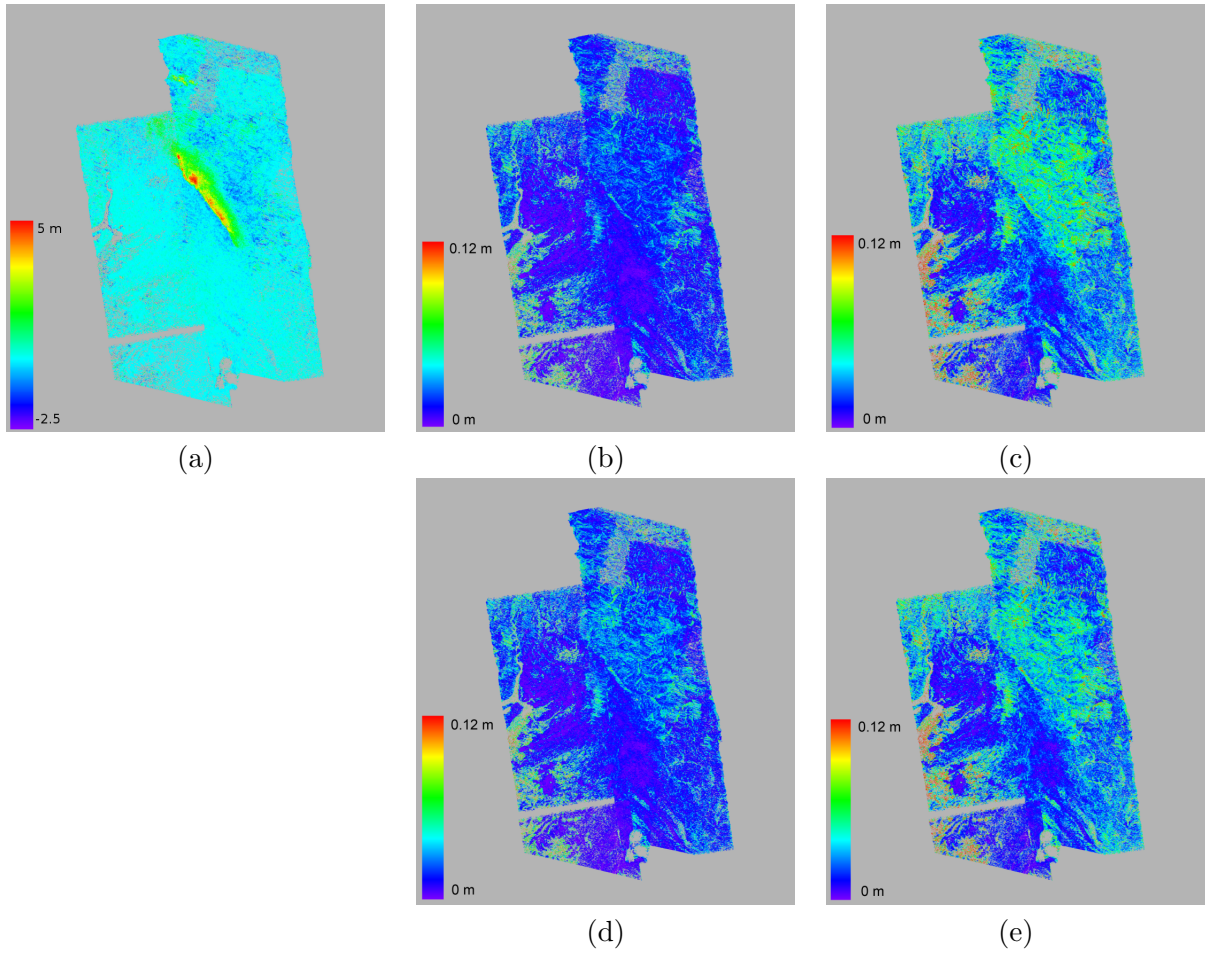
Figure 4: The Up component of the 3D displacement obtained with joint inversion (a) and the associated uncertainty obtained with (b) joint inversion, probabilistic approach (c) joint inversion, possibilistic approach (d) pre-fusion, probabilistic approach (e) pre-fusion, possibilistic approach in the case of the Kashmir earthquake in 2005.
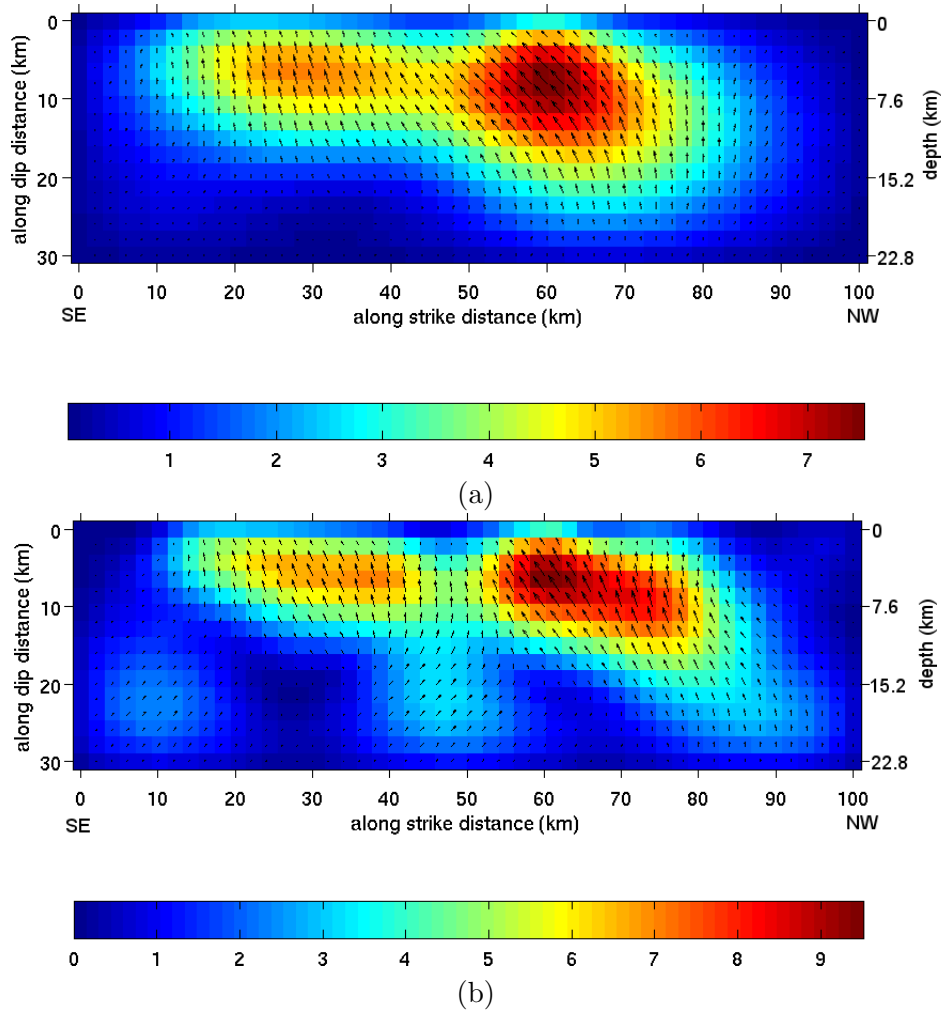
Figure 5: Slip distribution on the fault plane obtained with (a) pre-fusion (b) joint inversion for the Kashmir earthquake in 2005. The color represents the magnitude and the arrows represent the direction. Artefact is observed in depth in model (b) because of the difficulty in adjusting a model to a large number of noisy measurements.
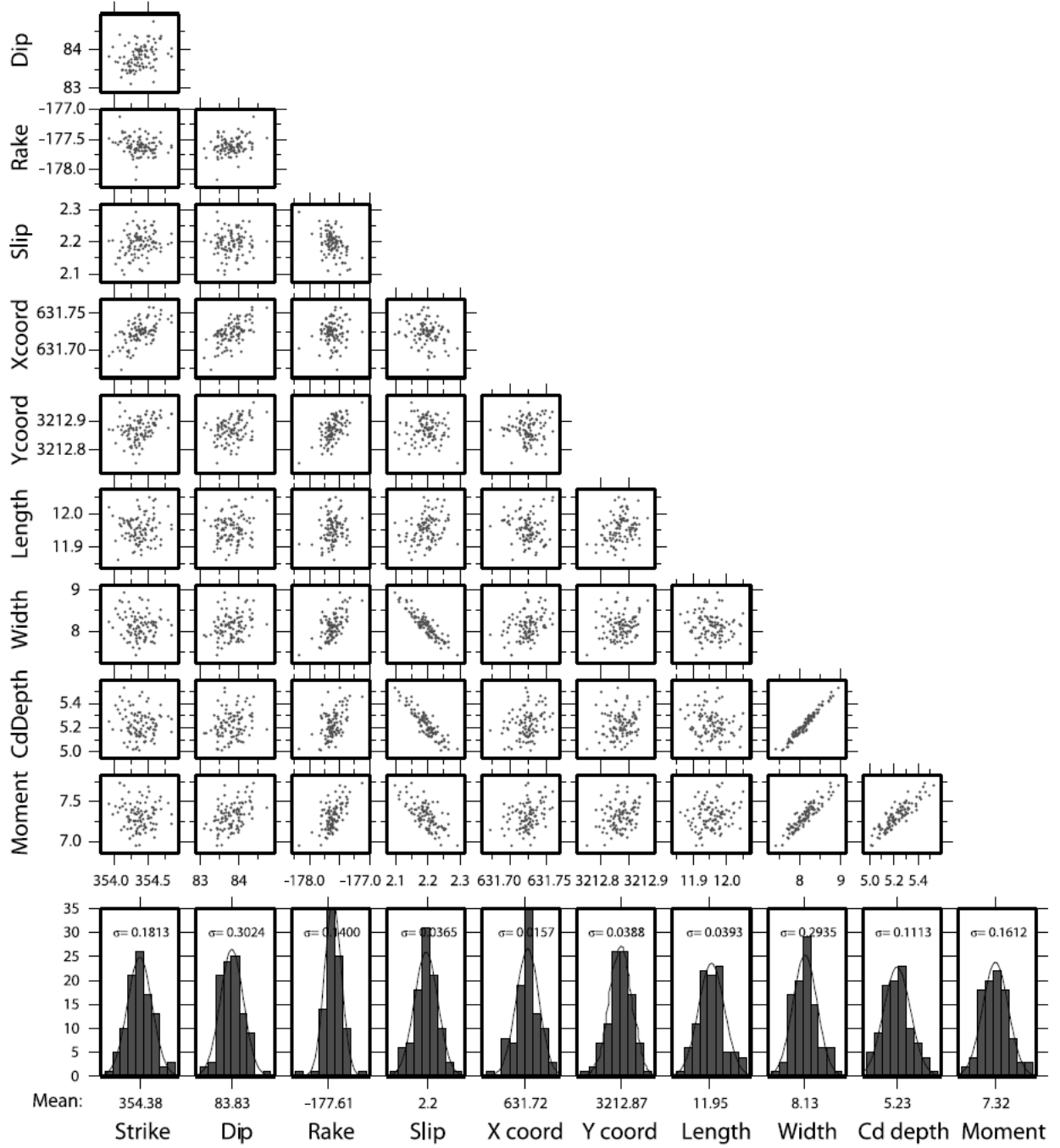
Figure 6: Example of distribution and correlation of geometrical parameters of a fault rupture model of the 2003 BAM (Iran) earthquake obtained by noise realisation (from [100]). Histograms show uncertainties in individual model parameters. Scatterplots show degrees of correlation (trade-off) between pairs of model parameters. (Strike, dip, and rake are in degrees; slip is in m; X and Y coordinates (of the centre of the fault plane projected updip to the surface) are in UTM km (zone 40); length, width, and centroid (Cd) depth are in km; and moment is in units of 1018 N m.)
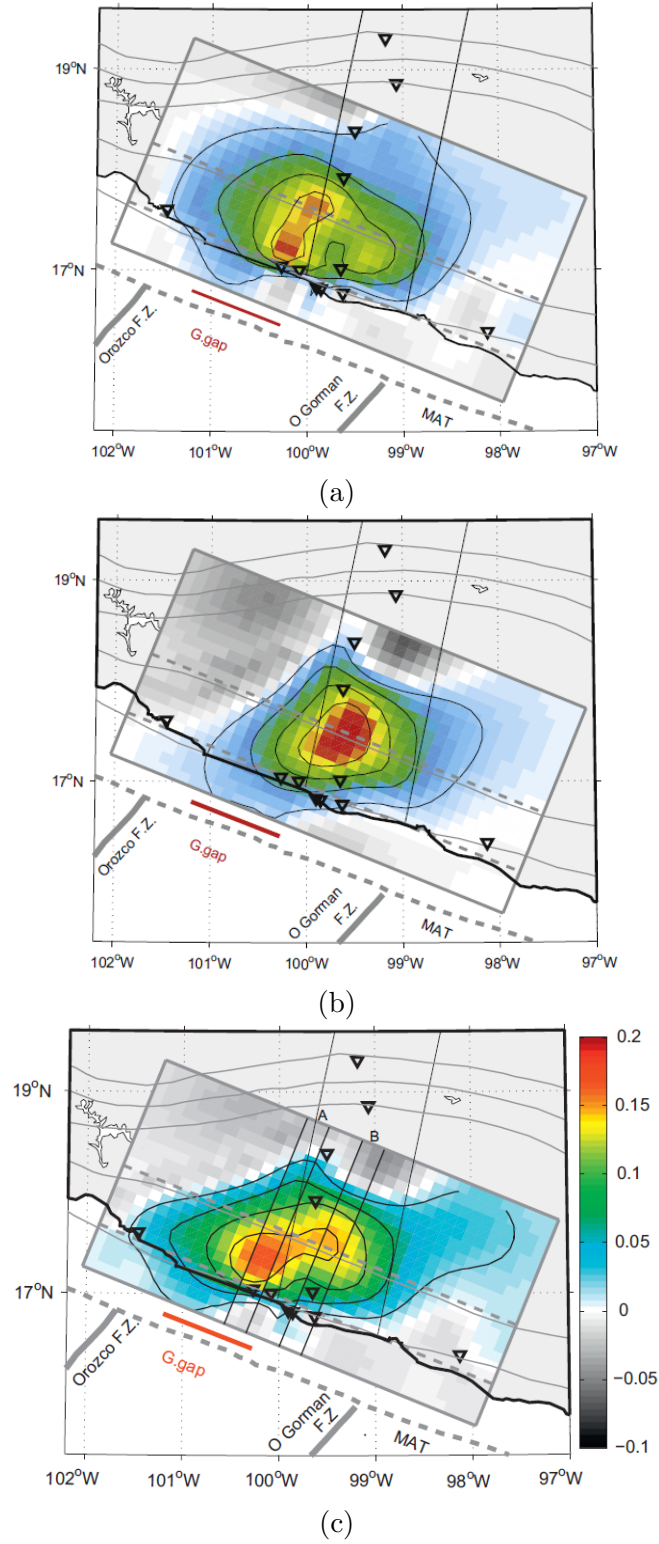
Figure 7: Slip model for the 2006 slow slip events in the Guerrero seismic gap inferred from (a) GPS measurement alone (b) InSAR measurements alone (c) joint minimisation of residual of both GPS and InSAR measurements (from [38]). GPS stations are represented by open black triangles and InSAR track by black box. Dashed thin gray lines indicate the changes in the dip of the model subduction plane. Dashed thick gray line represents the Middle American Trench (MAT) and thick continuous gray lines correspond to fracture zones. The location of the Guerrero gap (G.gap) is shown in red.

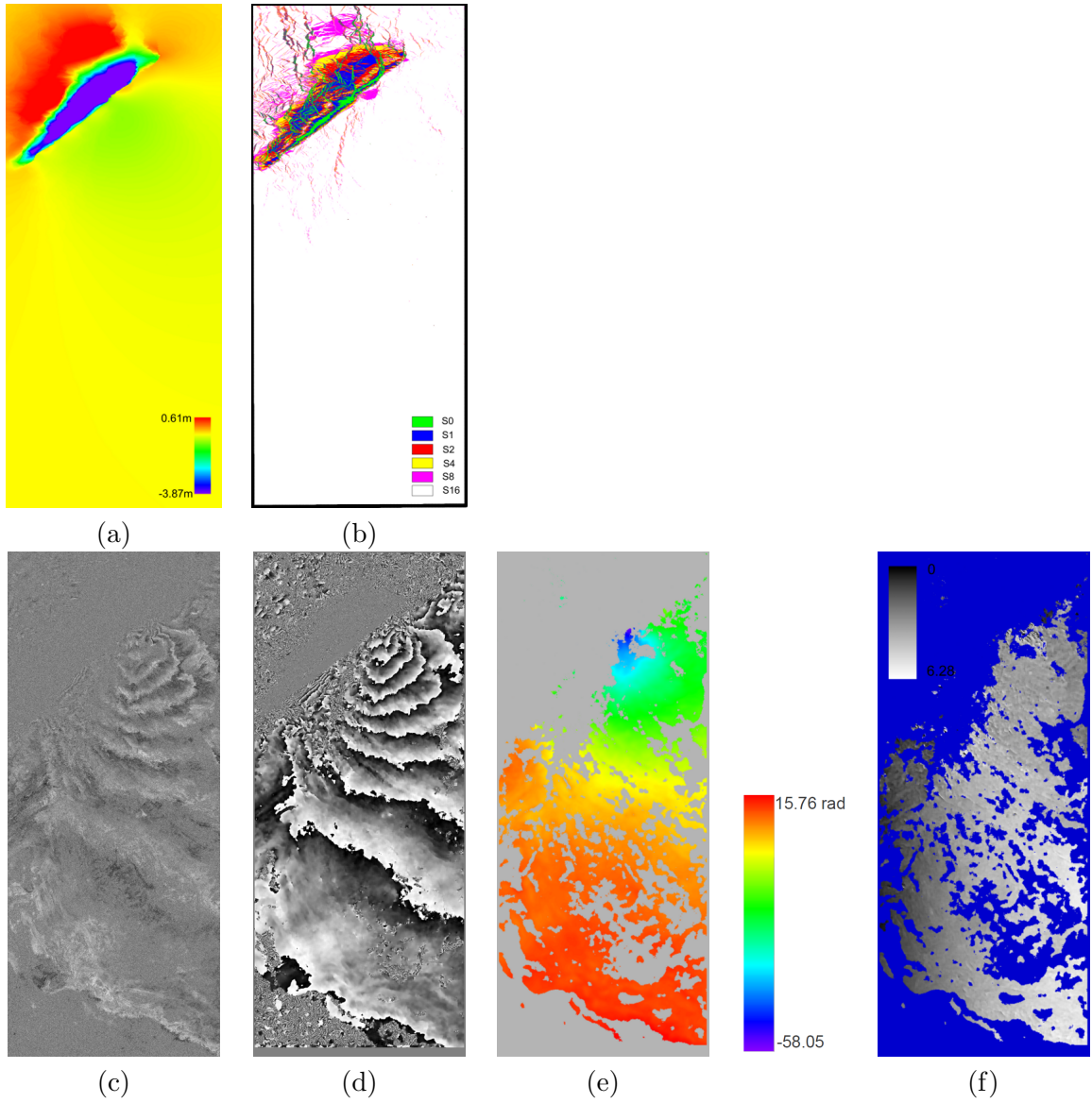(a)   (b)

(c)   (d)   (e)   (f)

Figure 8: (a) A priori deformation model in LOS direction, negative value for displacement towards the satellite. (b) Scale image for phase gradient estimation deduced from the a priori deformation model. S_0 corresponding to the full resolution SLC image and S_n to the multi-looking image after a complex average of n looks in range and $5n$ looks in azimuth. (c) Original differential interferogram (d) Filtered interferogram by multi-scale phase gradient (e) Unwrapped interferogram using multi-scale phase gradient by a least squares method (f) Wrapped phase residual in the case of the Kashmir earthquake (2005) (from [34]).

Length (km)	Width (km)	Top Depth[a] (km)	Strike (deg)	Dip (deg)	East[b] (km)	North[b] (km)	Rake (deg)	Slip (cm)
12.2 (0.4)	14.1 (0.7)	1.9 (0.2)	133 (2)	47 (1)	373.83 (1.38)	4691.29 (1.58)	−103 (2)	56 (2)

[a]Vertical depth of the fault top edge.
[b]East and North coordinates are in UTM-WGS84, zone 33, and refers to the center of the fault trace.
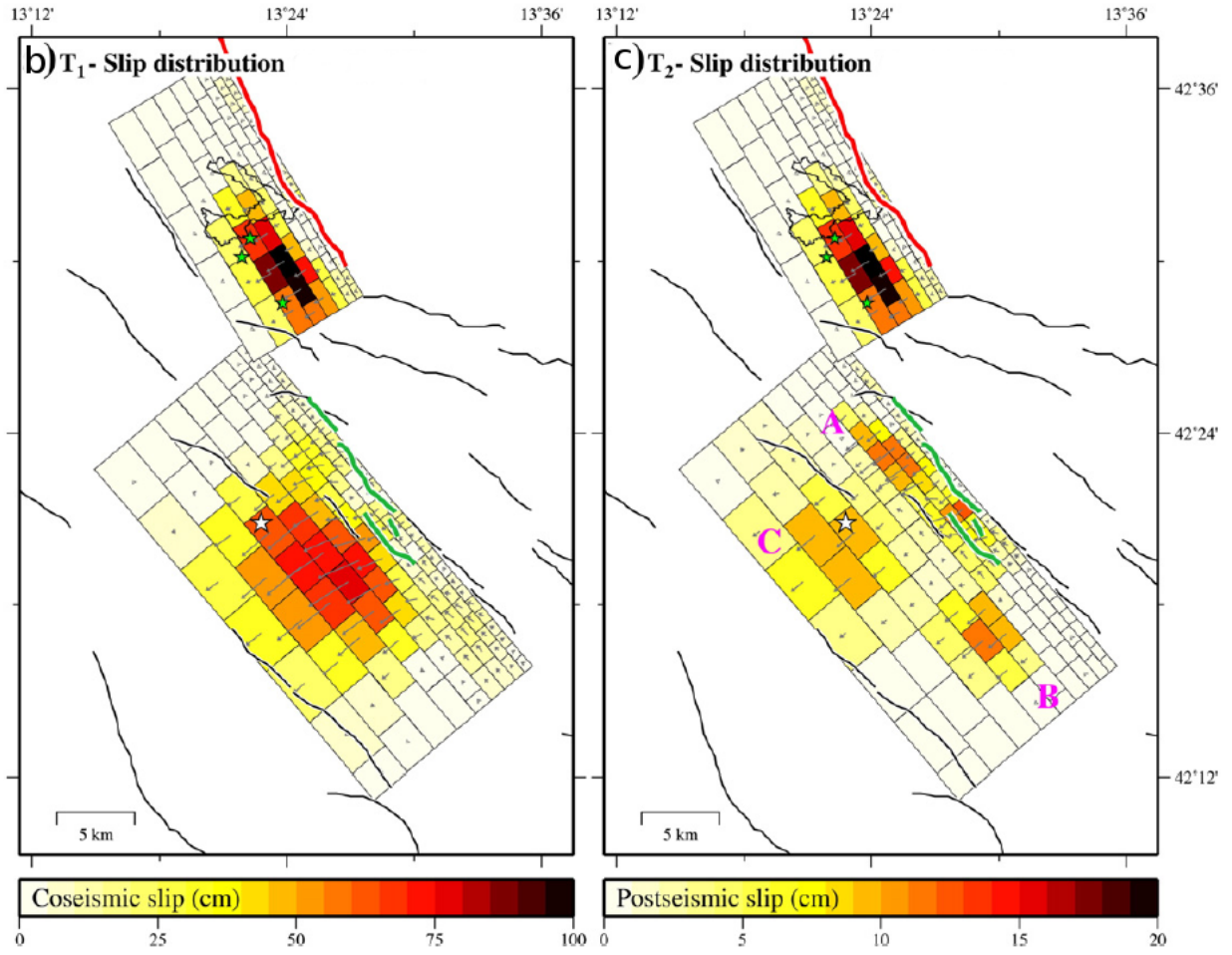
(a)

Figure 9: (a) Geometrical parameters of the Paganica fault estimated in [113] (b) Coseismic and (c) post-seismic slip distributions of the Paganica fault and the Campotosto fault using the Paganica fault geometry in (a) and the Campotosto fault geometry derived from geological mapping and InSAR, GPS and levelling data (from [15]). The write star indicates the April 6th Mw 6.3 L'Aquila mainshock, while the green stars are the three Mw > 5 aftershocks on the Campotosto fault. The Paganica fault is in green and the Campotosto fault is in red. The gray arrows show the slip direction.